Biochimica et Biophysica Acta 1850 (2015) 536–553

Contents lists available at ScienceDirect

Biochimica et Biophysica Acta

journal homepage: www.elsevier.com/locate/bbagen

Review

Bacteriorhodopsin: Would the real structural intermediates please stand up?☆

Cecilia Wickstrand [a], Robert Dods [a], Antoine Royant [b,c,d,e,*], Richard Neutze [a,*]

[a] Department of Chemistry and Molecular Biology, University of Gothenburg, Box 462, SE-40530 Gothenburg, Sweden
[b] Univ. Grenoble Alpes, IBS, F-38044 Grenoble, France
[c] CNRS, IBS, F-38044 Grenoble, France
[d] CEA, IBS, F-38044 Grenoble, France
[e] European Synchrotron Radiation Facility, F-38043 Grenoble, France

ARTICLE INFO

Article history:
Received 25 February 2014
Received in revised form 23 May 2014
Accepted 29 May 2014
Available online 8 June 2014

Keywords:
Bacteriorhodopsin
Structural intermediates
Proton pumping
Global structural analysis

ABSTRACT

Background: Bacteriorhodopsin (bR) is the simplest known light driven proton pump and has been heavily studied using structural methods: eighty four X-ray diffraction, six electron diffraction and three NMR structures of bR are deposited within the protein data bank. Twenty one X-ray structures report light induced structural changes and changes induced by mutation, changes in pH, thermal annealing or X-ray induced photo-reduction have also been examined.

Scope of review: We argue that light-induced structural changes that are replicated across several studies by independent research groups are those most likely to represent what is happening in reality. We present both internal distance matrix analyses that sort deposited bR structures into hierarchal trees, and difference Fourier analysis of deposited X-ray diffraction data.

Major conclusions: An internal distance matrix analysis separates most wild-type bR structures according to their different crystal forms, indicating how the protein's structure is influenced by crystallization conditions. A similar analysis clusters eleven studies of illuminated bR crystals as one branch of a hierarchal tree with reproducible movements of the extracellular portion of helix C towards helix G, and of the cytoplasmic portion of helix F away from helices A, B and G. All crystallographic data deposited for illuminated crystals show negative difference density on a water molecule (Wat402) that forms H-bonds to the retinal Schiff Base and two aspartate residues (Asp85, Asp212) in the bR resting state. Other recurring difference density features indicated reproducible side-chain, backbone and water molecule displacements. X-ray induced radiation damage also disorders Wat402 but acts via cleaving the head-groups of Asp85 and Asp212.

General significance: A remarkable level of agreement exists when deposited structures and crystallographic observations are viewed as a whole. From this agreement a unified picture of the structural mechanism of light-induced proton pumping by bR emerges. This article is part of a Special Issue entitled Structural biochemistry and biophysics of membrane proteins.

1. Introduction

Bacteriorhodopsin (bR) is the simplest known light driven proton pump. bR was discovered almost four decades ago in the purple membrane of *Halobacterium salinarum* [1] and was functionally characterized as a proton pump shortly afterwards [2,3]. Several other members of the bacterial rhodopsin family were later identified and functionally characterized, the first being halorhodopsin, which was initially suggested to be an outward directed sodium pump [4] but later characterized as an inward directed chloride pump [5]. Sensory rhodopsins were identified as photo-sensors that could guide their host towards favorable green light conditions and away from potentially damaging UV light [6]. A major breakthrough came with the discovery of oceanographic phototrophy mediated by proteorhodopsin [7], which is also a light driven proton pump very similar to bR. Genes encoding various proteorhodopsins have been identified in a large number of oceanographic bacteria and it has been suggested that rhodopsin mediated phototrophy is even more widespread in marine and terrestrial microbes than photosynthetic reaction centre mediated phototrophy [8]. Thus the proton pumping mechanism of the bacterial rhodopsin family is now recognized as a major pathway for harvesting the energy of sunlight within the marine environment.

☆ This article is part of a Special Issue entitled Structural biochemistry and biophysics of membrane proteins.

* Corresponding authors.
E-mail addresses: antoine.royant@ibs.fr (A. Royant), richard.neutze@chem.gu.se (R. Neutze).

http://dx.doi.org/10.1016/j.bbagen.2014.05.021

Because of its high stability and light-driven function, bR has long served as a model system in several spheres of biophysics. It has been characterized in detail using all forms of visible and vibrational spectroscopy [9]. When combined with site-directed mutagenesis, spectroscopic approaches have proven very powerful and the field has converged upon a widely accepted sequence of bR spectral intermediates (Fig. 1A) and the proton-exchange steps between key residues (Fig. 1B) [10]. Since proton pumping is ubiquitous in nature and the mechanism of chemiosmotic coupling underlies energy transduction within all spheres of life, a detailed understanding of the mechanism of proton pumping by bR impacts far beyond the specifics of the bR photocycle. In particular, the underlying principles of unidirectional proton pumping by bR are almost certainly relevant to the study of other proton pumps such as cytochrome c oxidase [11], ATP-synthase [12] and proton coupled transporters [13].

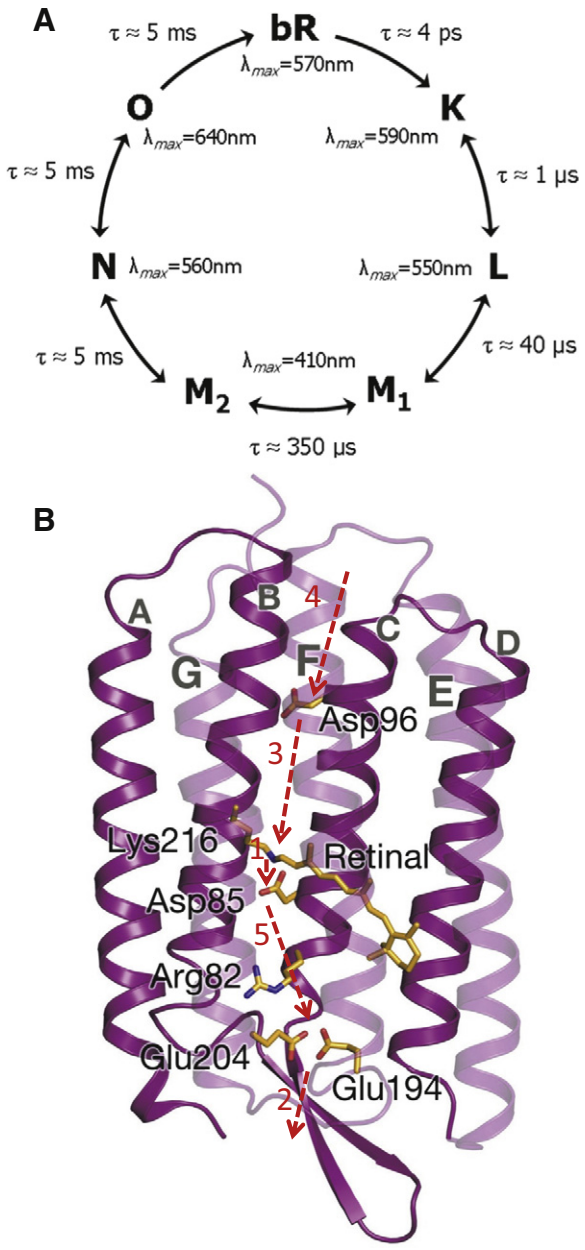

Fig. 1. Overview of the bR photo-cycle and the proton exchange steps. A, Photocycle of bR with the spectral intermediates (K to O) and their approximate time-scales. The absorption of a photon causes the all-*trans* retinal to be isomerized to a 13-*cis* configuration, driving a sequence of structural changes within the protein that lead to unidirectional proton transport. B, Seven transmembrane helical structure of bR, the location of key residues along the proton-translocation channel, and the accepted sequence of proton exchange events. Step 1: proton movement from the retinal SB to Asp85; Step 2: proton release to the extracellular space from the proton release group consisting of Glu194, Glu204 and water molecules; Step 3: reprotonation of the retinal SB from Asp96; Step 4: proton uptake from the cytoplasm; Step 5: deprotonation of Asp85 via proton exchange to the proton release group after the 13-*cis* retinal reisomerizes to its all-*trans* resting state configuration.
Reproduced with permission from Reference [93].

Function is closely coupled to protein structure and consequently considerable effort has gone into elucidating the structure of bR in its resting state, as well as the structures of its photo-cycle intermediates. The very first structural information for any membrane protein was obtained from bR to 7 Å resolution and emerged in 1975 using electron diffraction from the natural occurring 2D crystals of bR found within the purple membrane of *Halobacterium salinarum* [14]. A landmark contribution to the field was made 15 years later when the first atomic level model of bR [15] was also solved by electron diffraction. Since this time there has been an explosion of interest in the structural biology of bR, with eighty four X-ray diffraction, six electron diffraction and three NMR structures of bR now deposited in the protein data bank (Table 1). Many of these structures report conformational changes after treating crystals with light, pH changes, thermal annealing, X-ray photo-reduction, or after one or several residues were mutated. In most cases, the observed conformational changes were argued to be relevant to the mechanism of proton pumping by bR.

Twelve years ago we summarized the structural results that emerged from the first intermediate trapping studies on 3D crystals of bR [16–20] and bR mutants studied by X-ray [21] and electron diffraction [22]. We argued that structures solved at that time provided a consistent framework from which the mechanism of light-driven proton pumping by bR could be understood [23]. Numerous additional studies have been made since this time, often closely related to the first low-temperature trapping studies and often contradicting, or in other ways critical of, these early results. While experimental replication is essential to the scientific approach and is usually constructive as new details emerge with improving technology, the requirement for scientific novelty also creates pressure to emphasize differences rather than similarities with earlier work. For bR, a field that has never been shy of internal dissent [24], this large body of structural work (Table 1) may appear like a confusing maze of conflicting details: *one simply can't see the wood for the trees!*

To address this situation, we return to the structural mechanism of bR but examine the deposited crystal structures and crystallographic observations as one set of data, taking the view that *structural results reproducibly recovered by independent research groups are those most likely to represent what is happening in reality*. We organize this data by calculating a hierarchal tree based upon an internal-distance matrix analysis of the C_α atoms of deposited pdb structures [25]. When applied to the resting state structures of wild-type bR (of which there are thirty six structures; Table 1) this analysis, with very few exceptions, clusters the deposited crystal structures according to the space group in which they are crystallized, proving the point that no single "true bR structure" exists but rather the protein is influenced by the environment in which it is crystallized. When the same philosophy is applied to sort the light-induced changes, mutation induced changes, or other perturbations to the bR structure, we find that eleven of twenty one light-induced structural changes cluster as one branch of the hierarchal tree (Pearson correlation coefficient, PCC $\geq$ 0.597) whereas four (of the remaining ten) light-induced studies report K-intermediates and display very little C_α movement. A neighboring branch contains two structures of the bR D96G/F171C/F219L triple mutant proposed to mimic the later bR photocycle intermediates (PCC $\geq$ 0.5) whereas none of the pH, X-ray photo-reduced, xenon bound, or other mutation induced structural changes show similar movements on C_α atoms (PCC $\leq$ 0.35).

Local light induced changes were examined by calculating error weighted difference Fourier electron density maps from all deposited

Table 1
Structures of bR deposited in the protein data bank. Structures presented in references [116-130] are not analyzed further in this review.

PDB	SFs	Res. (Å)	Year [ref]	xtals	Notes*
1BRD	Yes	3.5	1990 [15]	PM	EM
2BRD		3.5	1996 [49]	PM	EM
1FBB		3.2	2000 [22]	PM	EM
1FBK		3.2	2000 [22]	PM	EM, D96G/F171C/F219L
1AT9		3.0	1997 [27]	PM	EM
2AT9		3.0	1999 [50]	PM	EM
1AP9	Yes	2.35	1997 [30]	LCP	
1QHJ	Yes	1.9	1999 [26]	LCP	
1QKO	Yes	2.1	1999 [16]	LCP	K-state
1QKP	Yes	2.1	1999 [16]	LCP	K-state
1E0P	Yes	2.1	2000 [18]	LCP	K:L:M (1:3:1)
1VJM	Yes	2.3	2004 [62]	LCP	L-state
1BRR	Yes	2.9	1998 [40]	HN	
1BRX		2.3	1998 [32]	LCP	
1C3W		1.55	1999 [33]	LCP	
1C8R		2.0	1999 [17]	LCP	D96N
1C8S		2.0	1999 [17]	LCP	M-state, D96N
1F4Z		1.8	2000 [20]	LCP	M-state, E204Q
1F50		1.7	2000 [20]	LCP	E204Q
1JV6		2.0	2001 [21]	LCP	D85S/F219L
1JV7		2.25	2001 [21]	LCP	D85S
3T45	Yes	3.0	2012 [116]	Bicelle	A215T
1M0K		1.43	2002 [64]	LCP	K-state
1M0L		1.47	2002 [64]	LCP	
1M0M		1.43	2002 [65]	LCP	M1-state
1O0A		1.62	2003 [66]	LCP	L-state
1P8H		1.52	2003 [67]	LCP	M1-state
1P8I		1.86	2003 [67]	LCP	F219L
1P8U		1.62	2003 [67]	LCP	N-state, V49A
2I1X	Yes	2.0	2006 [68]	LCP	D96A
2I20	Yes	2.08	2006 [68]	LCP	M-state D96A
2I21	Yes	1.84	2006 [68]	LCP	T46V
2NTU	Yes	1.53	2007 [69]	LCP	
2NTW	Yes	1.53	2007 [69]	LCP	L-state
1QM8		2.5	1998 [41]	VF	
1BM1		3.5	1999 [117]	VF	Light adapted
1IW6		2.3	2002 [57]	VF	
1IXF		2.6	2002 [57]	VF	K-state
1DZE		2.5	2004 [71]	VF	M-state
1IW9		2.5	2004 [71]	VF	M-state
1UCQ	Yes	2.4	2004 [70]	VF	L-state
1X0I	Yes	2.4	2005 [75]	VF	Acid blue
1X0K	Yes	2.6	2005 [75]	VF	Alkaline purple
1X0S	Yes	2.5	2005 [77]	VF	Dark adapted
2ZFE	Yes	2.5	2008 [76]	VF	Xenon-bound
2ZZL	Yes	2.03	2009 [72]	VF	M-state
3VHZ	Yes	2.3	2012 [73]	VF	L93A
3VI0	Yes	2.3	2012 [73]	VF	O-state, L93A
1CWQ		2.25	2000 [118]	LCP	M-state
1KG8		2.0	2001 [63]	LCP	M-state
1KG9		1.81	2001 [63]	LCP	Thawed & frozen
1KGB		1.65	2001 [63]	LCP	
1MGY		2.0	2003 [119]	LCP	D85S + Bromine
1S8J	Yes	2.3	2004 [120]	LCP	D85S + Nitrate
1S8L	Yes	2.3	2004 [120]	LCP	D85S
4FPD	Yes	2.65	2013 [74]	LCP	D96G/F171C/F219L
1L0M			2001 [47]		NMR
1R2N			2002 [46]		NMR
1R84			2002 [46]		NMR
1KME		2.0	2002 [42]	Bicelle	
1PXR		1.7	2004 [121]	Bicelle	P50A
1PXS		2.2	2004 [121]	Bicelle	M56A
1PY6		1.8	2004 [121]	Bicelle	
1Q5I		2.3	2004 [122]	Bicelle	P186A
1Q5J		2.1	2004 [122]	Bicelle	P91A
1S51		2.0	2004 [123]	Bicelle	T24S
1S52		2.3	2004 [123]	Bicelle	T24V
1S53		2.0	2004 [123]	Bicelle	T46S
1S54		2.2	2004 [123]	Bicelle	T24A
1TN0		2.5	2004 [124]	Bicelle	A51P
1TN5		2.2	2004 [124]	Bicelle	K41P
1XJI		2.2	2005 [43]	Bicelle	
3COC	Yes	2.31	2008 [125]	Bicelle	D115A
3COD	Yes	2.70	2008 [125]	Bicelle	T90A/D115A
3HAN	Yes	2.75	2009 [126]	Bicelle	V49A
3HAO	Yes	2.39	2009 [126]	Bicelle	L94A
3HAP	Yes	1.60	2009 [126]	Bicelle	L111A
3HAQ	Yes	2.30	2009 [126]	Bicelle	I148A
3HAR	Yes	1.70	2009 [126]	Bicelle	I148V
3HAS	Yes	1.90	2009 [126]	Bicelle	L152A
3UTV	Yes	2.06	2012 [127]	Bicelle	Y57F
3UTW	Yes	2.40	2012 [127]	Bicelle	P50A/Y57F
3UTX	Yes	2.47	2012 [127]	Bicelle	T46A
3UTY	Yes	2.37	2012 [127]	Bicelle	P50A/T46A
2WJK	Yes	2.3	2010 [128]	LCP	E204D
2WJL	Yes	2.15	2010 [128]	LCP	E194D
3MBV	Yes	2.0	2010 [129]	LCP	
3NS0	Yes	1.78	2011 [58]	LCP	
3NSB	Yes	1.78	2011 [58]	LCP	Radiation damaged
4MD1	Yes	1.73	2014 [78]	LCP	Orange species
4MD2	Yes	1.73	2014 [78]	LCP	
4HWL	Yes	2.0	2013 [130]	Bicelle	
4HYX	Yes	1.99	2013 [130]	Bicelle	

*Unless otherwise marked these are wild-type structures of bR
PM: Purple Membrane
LCP: Lipidic Cubic Phase
HN: Heterogeneous Nucleation
VF: Vesicle Fusion
Shading colour indicates structures from a group or collaboration.

data for which relevant excited state data (light induced) and reference (dark state) data have been deposited. A remarkable level of agreement is again observed, with all deposited data revealing that the key water molecule that bridges the retinal Schiff base (SB), Asp85 and Asp212 (referred to as Wat402 [26]) is disordered by exposure to light. Several other difference density features are reproducibly observed with varying significance and indicate movements of the Lys216 side-chain and backbone; movements of the side-chain of Arg82; movements of the Trp182 side-chain; and backbone movements of residues 82 to 85 of helix C. Difference density maps calculated from deposited data examining the influence of X-ray induced photo-reduction of bR also reveal a disordering of Wat402, but clearly show that the head-groups of Asp85 and Asp212 are cleaved by photo-reduction. Thus Wat402 is disordered by light induced retinal isomerization in one set of experiments, and by X-ray induced cleavage of the carboxylic groups of aspartic acid residues in another.

Taken together, this analysis demonstrates that an internal distance matrix based hierarchal sorting of deposited pdb entries provides a powerful tool for examining multiple structures as one set; that there is a high level of agreement concerning the light-induced movements of C_α atoms in bR; that all deposited crystallographic data concerning light-driven structural change in bR show disordering of Wat402 and reproducibly reveal other movements in the vicinity of the retinal; and while Wat402 can be disordered by X-ray induced photo-reduction, the mechanism of action is via the cleavage of Asp85 and Asp212 rather than retinal isomerization. We conclude that these data provide a consistent picture of the bR photocycle, in which Wat402 is the keystone needed to understand the molecular mechanism of proton pumping [23].

2. Crystal forms of bR

BR is an integral membrane protein that has been crystallized in multiple media using a broad variety of conditions (Table 1). The first structural information concerning bR utilized the remarkable property that bR naturally forms 2D crystals in the purple membrane of *H. salinarum*. Electron diffraction images were recorded from small fragments of these natural crystals and yielded the first bR structure to 7 Å resolution [14], later to 3.5 Å [15] and eventually to 3.0 Å [27] resolution. Notably, crystallographic phases were recovered directly in the 1990 electron diffraction structure of Henderson et al. [15] and all X-ray structures of bR since can trace their molecular replacement phases back to this work.

3D crystals of bR were first reported as early as 1980 [28] but could not be optimized to yield a high-resolution structure of bR given the technology available at the time. A major break-through for X-ray crystallography studies of bR came with the development of the method of lipidic cubic phase (LCP) membrane protein crystallization by Landau and Rosenbusch [29] who showed that bR crystals a few tens of microns across could grow in a semi-solid bicontinuous lipidic matrix formed by mixing samples of solubilized bR with the lipid monoolein and then dehydrating this matrix using salt. The first bR structure using these conditions [30] provided one of the first examples where synchrotron-based micro-crystallography was used to record X-ray diffraction data from very small crystals, which has since become a major area in synchrotron radiation research [31]. LCP crystal structures of bR were subsequently reported at increasing resolution [26,30,32,33]. These crystals grow as stacked 2D crystals and suffer from a crystal defect called merohedral twinning [32] whereby the orientation of each of the 2D sub-crystals relative to the c-axis can vary in a random way. The level of twinning varies from crystal to crystal and this defect may be closely related to the speed in which crystals grow [34]. Since its conception almost two decades ago, the LCP has become a very successful media for crystallizing integral membrane proteins [35,36]. A most striking success is that the LCP is now the crystallization method of choice for solving the structures of G protein-coupled receptors [37,38], which are a very large and important family of receptors [39] that were long regarded as extremely difficult structural targets.

Several other 3D crystal forms of bR have also been reported. One early success was the monoclinic crystal form of bR obtained by heterogeneous nucleation of detergent solubilized bR on organic crystals of benzamidine [40]. bR has also been crystallized through temperature induced collapse of vesicles, which leads to a crystal packing that is less dense than the LCP form. In this approach the purple membrane is incubated at high temperature in the presence of detergent and then cooled for crystallization [41]. A fourth approach was the development of lipidic bicelle crystallization, whereby bR is first prepared into bicelles: a lipid/detergent mixture that forms disk like objects that surround the membrane protein and which can be manipulated to stimulate crystal growth [42,43]. As with LCP crystallization, this bicelle approach has proven successful in the study of other integral membrane proteins [44] including G protein-coupled receptors [45].

All of the above 3D crystal forms of bR grow as stacked layers of 2D crystals with varying arrangements of molecules within the membrane plane. The bicelle crystal form packs adjacent bR molecules within any given 2D plane with an opposite orientation relative to the membrane, whereas the LCP packing of wild-type bR has the trimers arranged relative to each other in a manner that closely matches that observed for the native purple membrane, including the presence of several lipids [26].

Solution phase nuclear magnetic resonance (NMR) spectroscopy has also been used as a tool to study the structure of bR [46,47]. Because of difficulties in recovering solution phase NMR spectra from membrane proteins within a detergent micelle, the first of these studies used an innovative approach of synthesizing fragments of bR, solving the structures of each of these fragments individually and then stitching these fragments together using overlapping regions and a limited number of inter-helical distance constraints [47]. Another study recorded NMR spectra from the entire bR in solution [46], but the structural analysis focused upon determining the conformation of the retinal under different conditions of dark-adaption using distance constraints from an X-ray structure [40] to aid interpretation of the NMR spectra.

3. Hierarchal clustering analysis of wild-type bR resting structures

Table 1 summarizes all structures of bR deposited in the pdb. These structures are grouped according to the collaboration of scientists that deposited the structure, with each sub-group of structures being ordered according to the first structure deposited by each of these collaborations. When representing the data in this tabulated form it is striking that a tremendous amount of scientific effort has gone into understanding the structural biology of bR. One also observes a positive effect of increasingly stringent requirements from several journals that crystallographic observations be deposited before publication, cumulating in the protein data bank making the submission of experimental data mandatory from January 2008, since the practice of releasing experimental data had varied from group to group prior to this date. A third impression is that anyone who may seek to understand the structural biology of bR may simply be overwhelmed by the sheer wealth of structural information, making it difficult to judge where these structures are similar, where they differ, and to what extent any structural differences are significant?

To address this concern we develop here a hierarchal tree analysis that scores the similarities between any two bR structures based upon differences in their internal distances between C_α atoms [25] and clusters them according to this score. When examining similar structures a key advantage of an internal distance matrix analysis is that, unlike a root mean square difference (rmsd) analysis, this approach does not require that structures first be aligned upon each other. Moreover, *an internal distance matrix analysis contains information on both the amplitude and the direction of C_α displacements* and is therefore a better tool than rmsd for assigning conformational differences. This scoring algorithm proceeds by first selecting the protein domains of interest, and here we select all transmembrane α-helix domains (helices A to G) as defined by the header of pdb entry 1QHJ (TM A: 6–32; TM B: 37–58; TM C: 80–100; TM D: 105–127; TM E: 131–160; TM F:165–191; TM G: 201–224); the internal distance matrix between C_α atoms over this domain, $[C_\alpha]_i$, is then calculated for all pdb entries of interest;

the difference internal distance matrix between any two pdb entries is calculated by subtracting one internal distance matrix from the other, $\Delta[C_\alpha]_{ij} = [C_\alpha]_i - [C_\alpha]_j$ for pdb entries *i* and *j*; and the scoring function S_{ij} relating pdb entries *i* and *j* is calculated as the average of the absolute value of all elements within this difference internal distance matrix: $S_{ij} = \mathrm{Avg}(|\Delta[C_\alpha]_{ij}|)$. In cases for which one or more of the selected C_α atoms are not present in either of the two pdb files, S_{ij} is calculated for the subset of C_α atoms present in both structures. From the set of S_{ij} between all selected pdb entries, a hierarchal tree was drawn by sequentially clustering all pdb entries with their nearest neighbor (*ie.* selecting *i* and *j* corresponding to the smallest value of S_{ij}) using single linkage clustering in MATLAB [48] and plotted using dendrogram. For pdb files containing both a dark and an illuminated state in the same file (1X0I, 1QKP, 1P8H, 1O0A, 1M0M, 1M0K, 1CWQ) only the dark state was considered in this part of the analysis.

Fig. 2 shows the results of this sorting algorithm when applied to sort all the deposited pdb structures of wild-type bR. A very striking outcome of this analysis is that a clear majority of the X-ray structures of wild-type bR (26 of 29) are very similar, being grouped in the lower portion of the hierarchal tree with a threshold of the average internal difference matrix value $S_{ij} \leq 0.25$ Å (Fig. 2) relative to its nearest neighbor. Moreover, these structures of wild-type bR largely self-sort according to their crystallization media and space group. For example, the five bicelle crystal structures of wild-type bR from Bowie (1PY6, 1XJI, 1KME) and Zhang (4HYX, 4HWL) form a sub-group of very similar structures ($S_{ij} \leq 0.105$ Å); as do ten LCP structures from Gordeliy (3MBV, 3NS0, 4MD2), Glaeser (1KGB) and Lanyi (1O0A, 2NTU, 1M0K, 1P8H, 1M0L, 1M0M); and two LCP resting state structures from Landau also cluster below this threshold (1QHJ, 1QKP). A slight relaxation ($S_{ij} \leq 0.12$ Å) allows five wild type vesicle fusion structures from Kouyama to be clustered as a single group (1QM8, 1X0K, 1X0S, 2ZFE, 1IW6). This group joins the same branch of the hierarchal tree as almost all high resolution LCP structures of bR when a threshold of $S_{ij} \leq 0.20$ Å is applied, at which point this branch then also includes the crystal structure recovered by heterogeneous nucleation by Essen (1BRR). It is striking that one NMR structure (1R2N) clusters beside 1BRR within this group, but closer inspection of that work [46] reveals that this X-ray structure was used as a model to aid the interpretation of the NMR data and thus 1R2N cannot be regarded as a truly independent structure. Raising the bar to $S_{ij} \leq 0.25$ Å incorporates the 1.55 Å LCP structure of Luecke (1C3W), which is the most cited of any X-ray structure of bR; the LCP structure of Büldt (1CWQ); and the sub-branch of five bR structures solved from bicelle grown crystals mentioned above.

At the other end of the tree, pdb entry 1L0M differs most from all other structures of bR, which may have been anticipated since this NMR structure was solved by piecing together sub-structures of helical fragments of bR solved by NMR spectroscopy and then combing these into a single structure using a number of reasonable inter-helical

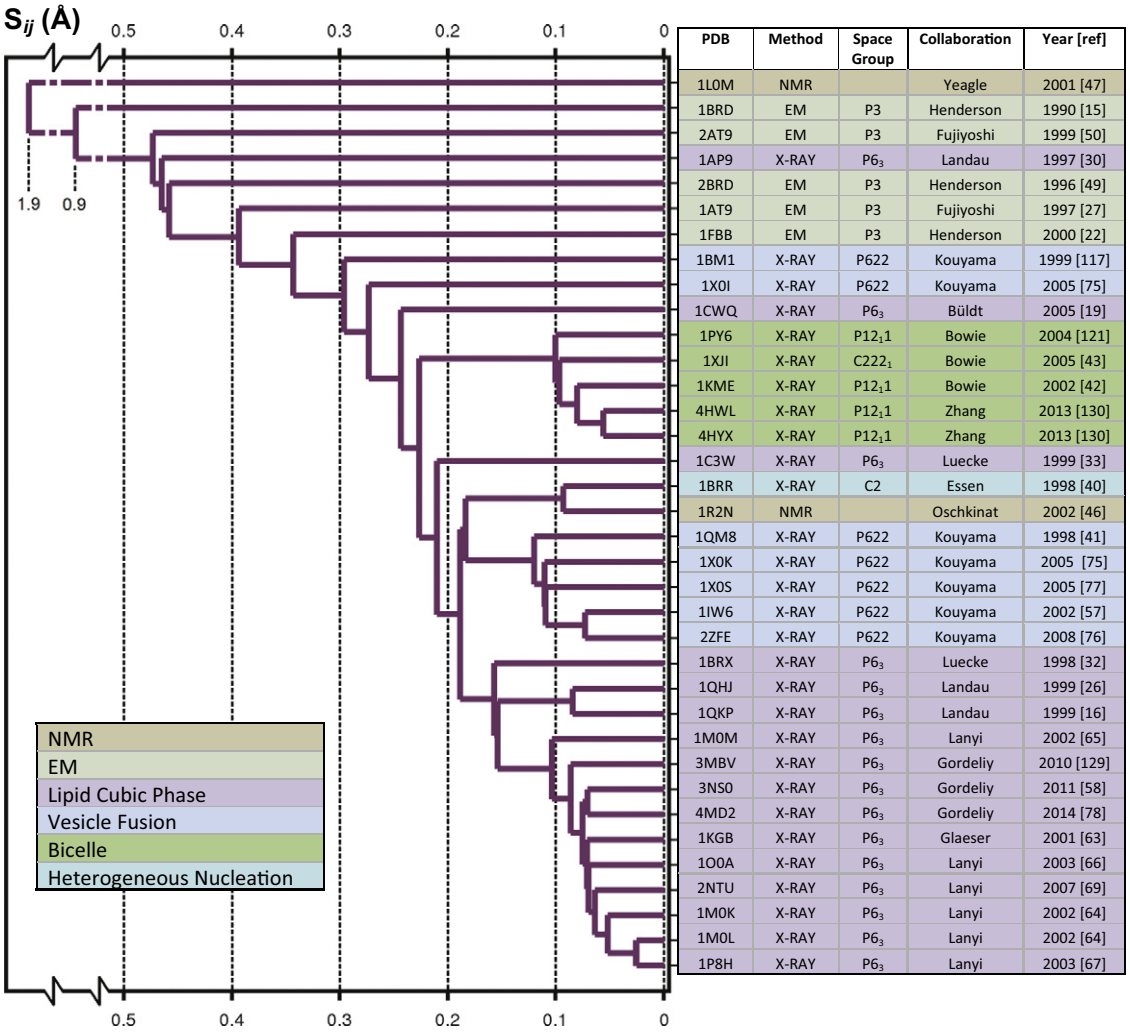

PDB	Method	Space Group	Collaboration	Year [ref]
1L0M	NMR		Yeagle	2001 [47]
1BRD	EM	P3	Henderson	1990 [15]
2AT9	EM	P3	Fujiyoshi	1999 [50]
1AP9	X-RAY	$P6_3$	Landau	1997 [30]
2BRD	EM	P3	Henderson	1996 [49]
1AT9	EM	P3	Fujiyoshi	1997 [27]
1FBB	EM	P3	Henderson	2000 [22]
1BM1	X-RAY	P622	Kouyama	1999 [117]
1X0I	X-RAY	P622	Kouyama	2005 [75]
1CWQ	X-RAY	$P6_3$	Büldt	2005 [19]
1PY6	X-RAY	$P12_11$	Bowie	2004 [121]
1XJI	X-RAY	$C222_1$	Bowie	2005 [43]
1KME	X-RAY	$P12_11$	Bowie	2002 [42]
4HWL	X-RAY	$P12_11$	Zhang	2013 [130]
4HYX	X-RAY	$P12_11$	Zhang	2013 [130]
1C3W	X-RAY	$P6_3$	Luecke	1999 [33]
1BRR	X-RAY	C2	Essen	1998 [40]
1R2N	NMR		Oschkinat	2002 [46]
1QM8	X-RAY	P622	Kouyama	1998 [41]
1X0K	X-RAY	P622	Kouyama	2005 [75]
1X0S	X-RAY	P622	Kouyama	2005 [77]
1IW6	X-RAY	P622	Kouyama	2002 [57]
2ZFE	X-RAY	P622	Kouyama	2008 [76]
1BRX	X-RAY	$P6_3$	Luecke	1998 [32]
1QHJ	X-RAY	$P6_3$	Landau	1999 [26]
1QKP	X-RAY	$P6_3$	Landau	1999 [16]
1M0M	X-RAY	$P6_3$	Lanyi	2002 [65]
3MBV	X-RAY	$P6_3$	Gordeliy	2010 [129]
3NS0	X-RAY	$P6_3$	Gordeliy	2011 [58]
4MD2	X-RAY	$P6_3$	Gordeliy	2014 [78]
1KGB	X-RAY	$P6_3$	Glaeser	2001 [63]
1O0A	X-RAY	$P6_3$	Lanyi	2003 [66]
2NTU	X-RAY	$P6_3$	Lanyi	2007 [69]
1M0K	X-RAY	$P6_3$	Lanyi	2002 [64]
1M0L	X-RAY	$P6_3$	Lanyi	2002 [64]
1P8H	X-RAY	$P6_3$	Lanyi	2003 [67]

Fig. 2. Hierarchal clustering analysis tree calculated from all deposited pdb entries describing the resting conformation of wild-type bR. This tree has been sorted according to the average of the difference internal distance matrix: $S_{ij} = \mathrm{Avg}(|\Delta[C_\alpha]_{ij}|)$ calculated as $\Delta[C_\alpha]_{ij} = [C_\alpha]_i - [C_\alpha]_j$ for pdb entries *i* and *j* where $[C_\alpha]$ is the internal distance matrix calculated on C_α atoms. It is striking that this analysis sorts the sub-branches largely according to the choice of crystallization media. These results are described in Section 3.

constraints [47]. A trend is also observed that structures solved by electron diffraction have, with time, become closer to the X-ray diffraction structures since the three wild-type bR structures from the Henderson group [15,22,49] and the two electron diffraction structures from Fujiyoshi [27,50], arrange chronologically with the most recent structures further down in the hierarchal tree. Similarly the first X-ray diffraction structure from Landau solved using microcrystals at a microfocus X-ray diffraction beamline [30], which pushed the state of the art at the time, differs significantly from all other X-ray structures of bR; whereas that solved two years later using larger crystals and more standard data collection approaches [26] clusters with all other LCP crystal structures of bR.

From these results it is apparent that a hierarchal sorting of wild type bR structures founded upon an internal distance matrix analysis is able to distinguish structures solved by electron diffraction and X-ray diffraction, arrange the electron diffraction structures from each group chronologically, and (to a very large extent) sort the X-ray diffraction crystal structures of bR according to the choice of crystallization approach. Thus this analysis clearly captures and represents information contained within the deposited structures in a manner reflecting a natural sorting of these structures, revealing similarities despite variations from structure-to-structure due to noise in any crystallographic analysis. We conclude that this approach of taking a step back and examining all thirty six deposited structures of wild-type bR as a single set reveals how the protein is influenced by the crystal packing and manner in which it crystallizes, even though the inter-helical loops that form crystal contacts are excluded from this structural analysis.

4. Intermediate trapping studies of bR

In 1998 Getzoff and colleagues published a low-temperature intermediate trapping study of the light-induced photo-isomerization of the p-hydroxycinnamic acid chromophore of photoactive yellow protein at 0.85 Å resolution [51]. In their coverage of this work, Essen and Oesterhelt commented that: “Unfortunately, it will probably be a long time before we have such an eagle-eyed view of rhodopsins or phytochromes” [52]. Others were more optimistic and the next two years saw rapid progress towards elucidating the nature of light driven structural changes in bR at high-resolution. A sequence of high-profile publications in quick succession [16,17,20] cumulated in a special issue of *Nature* in 2000 on bR [18,19,22] containing a very accessible commentary by Kühlbrandt [53].

Five of these studies combined X-ray diffraction with different approaches to illuminating 3D crystals of bR either at cryogenic-temperature [16,18] or during thawing followed by flash-freezing [17,19,20] (Table 2). The sixth study was an electron diffraction structure of the D96G/F171C/F219L triple-mutant of bR [22] for which considerable evidence existed that this combination of mutations induced a structural change [54] that mimicked features associated with the later phase of the bR photocycle [55]. In 2002 we summarized these findings and argued that a unified view of the evolution of structural changes in the bR photocycle had emerged from which the key ideas underpinning proton pumping could be understood [23].

Despite this early progress, there were certainly weaknesses in these first experiments. For example in the first M-state structure [17] large regions of the cytoplasmic portions of helices E and F were simply missing from the model and these are the regions believed to undergo the largest conformational changes [54,55]; merohedral twinning lowered the quality of the difference Fourier electron density maps [19]; highly twinned data could not be detwinned [56] prior to further crystallographic analysis [17,20], which both increased phase bias during structural refinement and prevented the presentation of difference Fourier electron density maps; concerns emerged about X-ray induced radiation damage in the early studies [57,58]; and the extent to which the triple mutant structure [22] accurately represents light induced structural changes in the bR photocycle is something of a matter of faith. The most criticized study [59,60] was our publication concerning the L-intermediate of bR [18] because the spectral evidence we presented showed contamination from the M-intermediate: we were, quite simply, overconfident of the quality of the crystallographic data and did not address spectral concerns to the standard required. We responded with a more careful spectral characterization [61] demonstrating that our original trapping protocol yielded a 1:3:1 mixture of K:L:M, and we later repeated the experiment under conditions yielding a pure L-state [62]. Nevertheless, these controversies decreased the broader acceptance of the functional significance of these first intermediate trapping experiments and motivated further investigations of structural changes in bR.

Despite these controversies, it cannot escape attention that the thirteen intermediate trapping studies that sought to address the same questions [57,62–73] were very similar to the five trapping experiments that they followed [16–20] (Table 2). For example all three K-state studies [16,57,64] illuminated 3D crystals with green light at either 100 K or 110 K, although Kouyama sought to deplete K and recover the bR state using red light as part of their data collection protocol [57]; all five L-state studies used trapping protocols with crystals illuminated at 150 K [62], 160 K [70] or 170 K [18,66,69] using green [18,70] or red light [62,66,69], although Kouyama again sought to deplete the

Table 2
Intermediate trapping protocols used to investigate light driven structural change in bR.

PDB	Trapped state	Trapping protocol	Group	Year [ref]
1QKO/1QKP	K	Green light (532 nm) during data collection at 110 K.	Landau	1999 [16]
1E0P	K:L:M (1:3:1)	30 s green light (532 nm) at 170 K; data collection 110 K.	Landau	2000 [18]
1VJM	L	30 s red light (635 nm) at 150 K; data collection 110 K.	Landau	2004 [62]
1C8S	M (D96N)	Yellow light (>520 nm) during 3 s thawing*; data collection 100 K	Luecke	1999 [17]
1F4Z	M (E204Q)	Yellow light (594 nm) during 1 s thawing*; data collection 100 K	Luecke	2000 [20]
1CWQ	M	Green light (514 nm) during 1 s thawing*; data collection 95 K	Büldt	2000 [19]
1KG8	M	Yellow light (>515 nm) illumination at 230 K; data collection 100 K	Glaeser	2001 [63]
1M0K	K	Green light (532 nm) during data collection at 100 K	Lanyi	2002 [64]
1M0M	M1	Yellow light (594 nm) at 210 K; data collection at 100 K	Lanyi	2002 [65]
1O0A	L	60 s red light (633 nm) at 170 K; data collection at 100 K	Lanyi	2003 [66]
1P8H	M1	Yellow light (594 nm) during 3 s thawing*; data collection 100 K	Lanyi	2003 [67]
1P8U	N (V49A)	Red light (628 nm) during 3 s thawing*; data collection 100 K	Lanyi	2003 [67]
2I20	M (D96A)	Red light (628 nm) during 3 s thawing*; data collection 100 K	Lanyi	2006 [68]
2NTW	L	Red light (633 nm) at 170 K; data collection at 100 K	Lanyi	2007[69]
1IXF	K	Alternate red (678 nm, bR state) & green light (532 nm, K-state) at 100 K	Kouyama	2002 [57]
1UCQ	L	Green light (532 nm) at 160 K followed by red light (678 nm) at 100 K	Kouyama	2004 [70]
1DZE/1IW9	M	Orange light (540 to 700 nm) at 293 K; data collection 100 K	Kouyama	2004 [71]
2ZZL	M	Orange light (>540 nm) at 293 K; data collection 100 K	Kouyama	2009 [72]
3VI0	O (L93A)	Green light (532 nm) at 293 K; data collection 100 K	Kouyama	2012 [73]

* Thawing refers to a bR crystal being placed in a nitrogen gas stream at 100 K (or 95 K) and this gas stream being blocked for the specified time.

K-state by illuminating with red light after cooling to 100 K [70]; photostationary populations of the M-state were trapped using continuous illumination with yellow light at 210 K [65] or 230 K [63], or using orange light at 293 K [71,72] in a crystal form for which the bR photocycle is dramatically slowed [71,72]; the trick of illuminating bR crystals during thawing by blocking the cryo-stream for a few seconds was repeatedly used to trap the M [17,19,20,67,68] and N [67] photocycle intermediates; and the O intermediate was also trapped at 293 K using green light illumination [73].

X-ray structures were also reported for bR mutants believed to mimic photo-intermediates. For example Glaeser [74] determined the X-ray structure of the bR D96G/F171C/F219L triple-mutant previously solved by electron diffraction [22] and Luecke investigated structures of the D85S and D85S/F219L double bR mutant [21] argued to mimic the O-intermediate of bR, a photocycle intermediate which has D85 protonated. Other physical perturbations have also been investigated such as extremely low (acid blue) and high (alkaline purple) pH [75]; mock trapping (*ie.* heating and cooling of bR crystals without illumination [63]); the binding of xenon [76]; dark adaption [77]; and X-ray induced damage [58,78]. Thus, over the last 15 years a considerable body of work has emerged that reports structural changes in bR, yet each publication tended to highlight differences, rather than similarities, with earlier work. To identify similarities across separate studies we again take a step back and, as with our analysis of the wild-type bR structures above (Fig. 2), we examine these deposited structures as a single set.

5. Hierarchal tree of structural perturbations

Given this wealth of data on how the bR structure is affected by light, mutation or other physical perturbations we ask: *what C_α movements have been reproducibly observed and which of these are uniquely light-induced?* To this end we adapt the internal distance matrix analysis presented above that identified similarities and differences between two pdb entries of wild-type bR, to now identify similarities and differences between two pairs of pdb entries (excited versus resting). This extension is rather straightforward and, in practice, the only change required is to the choice of scoring function.

Again we begin by selecting all transmembrane α-helix domains (TM A: 6–32; TM B: 37–58; TM C: 80–100; TM D: 105–127; TM E: 131–160; TM F:165–191; TM G:201–224). For each pdb file of interest $(\text{pdb}^{\text{excited}})_i$ we identify the corresponding resting bR state $(\text{pdb}^{\text{resting}})_i$, which can usually be extracted from the original publication or the pdb entry. The difference internal distance matrix is then calculated as: $\Delta[C_\alpha]_i = [C_\alpha^{\text{excited}}]_i - [C_\alpha^{\text{resting}}]_i$. In this case the function $S_i(\Delta[C_\alpha]_i) = \text{Avg}(|\,[C_\alpha^{\text{excited}}]_i - [C_\alpha^{\text{resting}}]_i\,|)$ gives a measure, in units of Å, of the average change in internal distances when moving from the resting to the excited state. Although it contains some information (tabulated as S_i in Fig. 3), it is not used to draw the hierarchal tree. Instead we calculate the Pearson correlation coefficient (PCC) which relates two difference internal distance matrices: $\text{PCC}_{ij} = \text{PCC}(\Delta[C_\alpha]_i, \Delta[C_\alpha]_j)$ *and this function scores the similarities for how the bR structure changes when moving from the resting state to the excited state.* In cases where one or

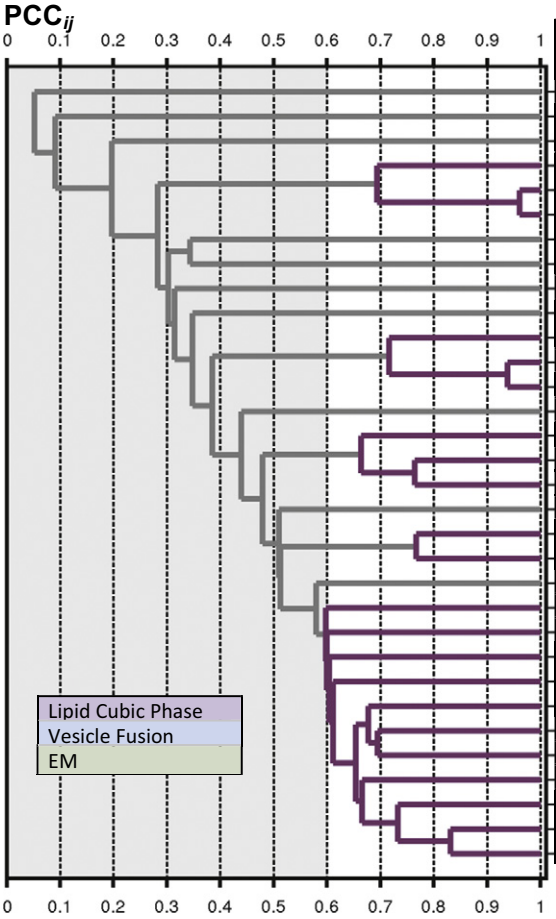

PDB	Ground state	Notes: K, L, M, N & O are illuminated	S_i(Å)	Collaboration	Year [ref]
4MD1	4MD2	Orange species	0.001	Gordeliy	2014 [78]
1M0K	1M0K	K	0.0005	Lanyi	2002 [64]
1IXF	1IW6	K	0.06	Kouyama	2002 [57]
1X0I	1IW6	Acid blue (pH 2)	0.28	Kouyama	2005 [75]
1JV6	1BRX	D85S/F219L	0.49	Luecke	2001 [21]
1JV7	1BRX	D85S	0.53	Luecke	2001 [21]
1X0K	1IW6	Alkaline (pH 10)	0.13	Kouyama	2005 [75]
2ZFE	1IW6	Xenon-bound	0.07	Kouyama	2008 [76]
3NSB	3NS0	X-ray damaged	0.14	Gordeliy	2011 [58]
1X0S	1IW6	Dark adapted	0.11	Kouyama	2005 [77]
1M0M	1M0M	M1	0.002	Lanyi	2002 [65]
1QKO	1QKP	K	0.01	Landau	1999 [16]
1QKP	1QKP	K	0.005	Landau	1999 [16]
1UCQ	1IW6	L	0.11	Kouyama	2004 [70]
1P8U	1P8U	N (V49A)	0.39	Lanyi	2003 [67]
1O0A	1O0A	L	0.23	Lanyi	2003 [66]
1P8H	1P8H	M1	0.19	Lanyi	2003 [67]
1KG9	1KGB	Annealed	0.10	Glaeser	2001 [63]
1FBK	1FBB	D96G/F171C/F219L	0.51	Henderson	2000 [22]
4FPD	1KGB	D96G/F171C/F219L	0.60	Glaeser	2013 [74]
1C8S	1C8R	M (D96N)	0.29	Luecke	1999 [17]
2NTW	2NTU	L	0.06	Lanyi	2007[69]
1CWQ	1CWQ	M	0.48	Büldt	2000 [19]
2I20	2I1X	M (D96A)	0.19	Lanyi	2006 [68]
1F4Z	1F50	M (E204Q)	0.24	Luecke	2000 [20]
1KG8	1KGB	M	0.19	Glaeser	2001 [63]
1E0P	1QHJ	K:L:M (1:3:1)	0.23	Landau	2000 [18]
1VJM	1QHJ	L	0.28	Landau	2004 [62]
3VI0	3VHZ	O (L93A)	0.14	Kouyama	2012 [73]
1DZE	1IW6	M	0.16	Kouyama	2004 [71]
1IW9	1IW6	M	0.17	Kouyama	2004 [71]
2ZZL	1IW6	M	0.17	Kouyama	2009 [72]

Fig. 3. Hierarchal clustering analysis tree for structural changes in bR induced by light, mutation, pH, xenon, thermal annealing, dark adaption and radiation damage. This tree has been sorted according to the Pearson correlation coefficient: $\text{PCC}_{ij} = \text{PCC}(\Delta[C_\alpha]_i, \Delta[C_\alpha]_j)$, where $\Delta[C_\alpha]_i$ is the change in internal distance matrix when moving from the resting to perturbed bR structure. Five main branches are observed and are described in detail in Section 5. Eleven of twenty one structures of light-induced structural changes in bR cluster within the final branch of this tree. White background indicates $\text{PCC}_{ij} \geq 0.597$ which has been used as a clustering cut-off throughout the discussion.

more of the selected C_α atoms are not present in any one of the four relevant pdb files (two excited, two resting), PCC_{ij} is calculated for the subset of C_α atoms present in all four structures. From the complete set of PCC_{ij} relating all relevant pdb entries, a hierarchal tree is drawn by sequentially clustering these pairs with their nearest neighbors (*ie.* selecting *i* and *j* with PCC_{ij} closest to 1) using single linkage clustering in MATLAB [48] and plotted using dendrogram.

Why do we adopt PCC_{ij} here whereas we used S_{ij} to sort the wild-type bR hierarchal tree? The answer is that *PCC_{ij} maintains the information on the nature and direction of the C_α movements.* For example, should a movement of a portion of helix C towards helix G be observed in two pairs of pdb entries: $(pdb^{excited}–pdb^{resting})_i$ and $(pdb^{excited}–pdb^{resting})_j$ then *PCC_{ij}* would yield a positive correlation. On the other hand should one pair show this movement of helices *towards* each other but another pair shows this movement *away* from each other, this would yield a negative *PCC_{ij}* correlation. Similarly, movements of helix A relative to F are not directly correlated with movements of helix C relative to G when using PCC_{ij}, whereas both would increase the value of $S_i(\Delta C_i)$. Another important point is that PCC_{ij} is largely independent of the amplitude of the movement, which reduces its sensitivity to assumptions concerning the crystallographic occupancy of an intermediate state made as different authors refined intermediate structures against their crystallographic data.

Fig. 3 presents the resulting hierarchal tree. As with our analysis of the wild-type bR structures (Fig. 2), it is striking how the branches of this tree reveal similarities and differences between these crystallographic studies. In particular, threshold of PCC ≥ 0.597 (white region, Fig. 3) neatly sub-divides this tree into five distinctive branches, each of which contains two or more related structures.

Beginning from the top of this tree, which corresponds to the cluster most removed from all other clusters, we find a three pronged branch containing both the D85S single mutation (1JV6–1BRX) and the D85S/F219L double mutation (1JV7–1BRX). These mutants were proposed to be analogues to the bR O-intermediate [21] and crystallize in the space group $C222_1$ rather than the hexagonal $P6_3$ LCP form of wild-type bR. Strikingly, our sorting algorithm places the acid-blue crystal structure of bR (1XOI–1IW6 [75]), which was crystallized at pH 2.0 and therefore had D85 protonated, in the same branch as these mutants, strongly supporting the argument of Luecke [21] that the D85S mutation mimics a bR state with D85 protonated. Nevertheless, these structures are far removed from the X-ray structure of the O-intermediate of Kouyama (3VI0–3VHZ, [73]). Moreover, the nature of the common conformational change can be extracted by examining the principle single value decomposition (SVD) component of these three difference internal distance matrices, which reveals a movement of the extracellular portions of helices D and E away from helices A, B, C, F and G (Fig. 4A). Thus, while the X-ray structures of the D85S, D85S/F219L and acid blue forms of bR are high quality and interesting crystallographic studies, they appear to have limited relevance to light driven structural changes during the bR photocycle.

The next cluster is formed by two K-intermediate pdb entries (1QKO–$1QKP_{gnd}$; $1QKP_{exc}$–$1QKP_{gnd}$; where "exc" denominates a light-activated state and "gnd" denominates the resting sate when a pdb entry contains both intermediate and resting structures [16]) and one M-intermediate study ($1M0M_{exc}$–$1M0M_{gnd}$ [65]). What is striking about this cluster is that the average change in distance between C_α atoms is perturbed only very slightly, $S_i(\Delta C_i) \leq 0.01$ Å for all three entries, and this is an order of magnitude lower than typically seen when comparing independent wild-type bR structures (Fig. 2). This is due to the fact that the resting and excited state models were not independent but rather only a limited number of residues were refined with dual occupancy to recover their resting and intermediate state conformations. This leads to a very distinctive difference internal distance matrix showing vertical and horizontal bands associated with the residuals in helices C (84–86) and G (212, 215–216) that were given freedom to move (Fig. 4B). For our K-intermediate study we motivated this conservative refinement protocol by presenting an overview of the difference Fourier electron density map [16] which showed only local electron density changes near the retinal. Although the two other K-state structures do not cluster with this set, they all show very small light-induced C_α-atom perturbations: the K-intermediate of Lanyi [64] having $S(1M0K_{exc}–1M0K_{gnd}) = 0.0005$ Å; that of Kouyama [57] having S(1IXF-1IW6) = 0.06 Å; and from our K-state refinements [16] $S(1QKO–1QKP_{gnd}) = 0.01$ Å and $S(1QKP_{exc}–1QKP_{gnd}) = 0.005$ Å. These results make physical sense since all K-states were trapped at 100 K or 110 K (Table 2) and protein motions are very restricted at this temperature [79]. The M1-state of Lanyi (1M0M) is exceptional since the average change of internal distances for C_α atoms, $S(1M0M_{exc}–1M0M_{gnd}) = 0.002$ Å and this is two orders of magnitude smaller than that recovered for all other deposited M-state structures (Fig. 3). It is therefore difficult to know how to interpret this M1-state structure and regrettable that no difference Fourier map was presented to motivate the restricted structural refinement protocol [65].

The next sub-branch of this hierarchal tree consists of three studies of photo-activated bR, all of which were solved by the same group: an L-state ($1O0A_{exc}$–$1O0A_{gnd}$ [66]); an M1-state ($1P8H_{exc}$–$1P8H_{gnd}$ [67]) and an N-state ($1P8U_{exc}$–$1P8U_{gnd}$ [67]) where the latter is trapped using the V49A bR mutant. All three structures show significant changes in internal distances on C_α atoms with $0.19 \text{ Å} \leq S(1P8H_{exc}–1P8H_{gnd}) \leq S(1O0A_{exc}–1O0A_{gnd}) \leq S(1P8U_{exc}–1P8U_{gnd}) \leq 0.39$ Å. An SVD analysis of the resulting internal distance matrix changes reveals the nature of this recurring conformational perturbation, whereby the principal component displays a pattern resembling a checkerboard tilted by 45° (Fig. 4C). This tilted checkerboard corresponds physically to the distances between the extracellular and cytoplasmic portions of the bR structure systematically decreasing. Is it possible that photoactivation of bR shrinks the protein and these authors have discovered an unknown global conformational change critical to the mechanism of proton pumping? This seems unlikely since this checkerboard pattern is also recovered when comparing the wild-type resting bR structures from Luecke (1C3W) and Lanyi ($1O0A_{gnd}$) (Fig. 4D). We note that pdb entries 1O0A, 1P8H and 1P8U all have a c-axis approximately 3 Å shorter than earlier bR structures from the same group (1M0K, 1M0L, 1M0M, Table 1) and a similar checkerboard pattern can be generated if one refines two bR structures against the same data but with the c-axis arbitrarily shortened in one case. These observations indicate that this apparent compression may stem from slight errors in determining the crystallographic c-axis.

Proceeding down the tree, we reach a sub-branch consisting of two structures of the D96G/F171C/F219L triple mutant independently solved by electron diffraction (1FBK–1FBB [22]) and X-ray crystallography (4FPD–1KGB [74]). These pdb entries display some of the largest structural perturbations, having an average internal distance matrix change $S(1FBK–1FBB) = 0.60$ Å and $S(4FPD–1KGB) = 0.51$ Å. Examining the principle SVD component of these two difference internal distance matrices (Fig. 4E) shows that structural changes common to both studies consist of significant movements of the cytoplasmic side of helix F away from helices A, B, C, D and G. This branch sits adjacent to the main group of light activated structures (2NTW to 2ZZL, Fig. 3) and supports the hypothesis that these three mutations combined induce a conformational change which, to some extent, mimics light activated changes in bR [7,54,55]. Moreover, this is the first sub-branch of the hierarchal tree to be placed closer to the main branch of light-induced conformational changes than the mock trapping study by Glaeser (1KG9–1KGB [63]) for which bR crystals were heated and cooled but were not illuminated.

Finally we arrive at the main branch of light-induced conformation changes in bR. Allowing a (somewhat arbitrary) threshold of $PCC_{ij} \geq 0.597$ defines a set of eleven paired pdb entries, all of which concern studies of light-induced structural changes in 3D bR crystals illuminated at temperatures ranging from 150 K to 293 K, include structures of L, M and O states (Table 2). This set of studies incorporates structures from

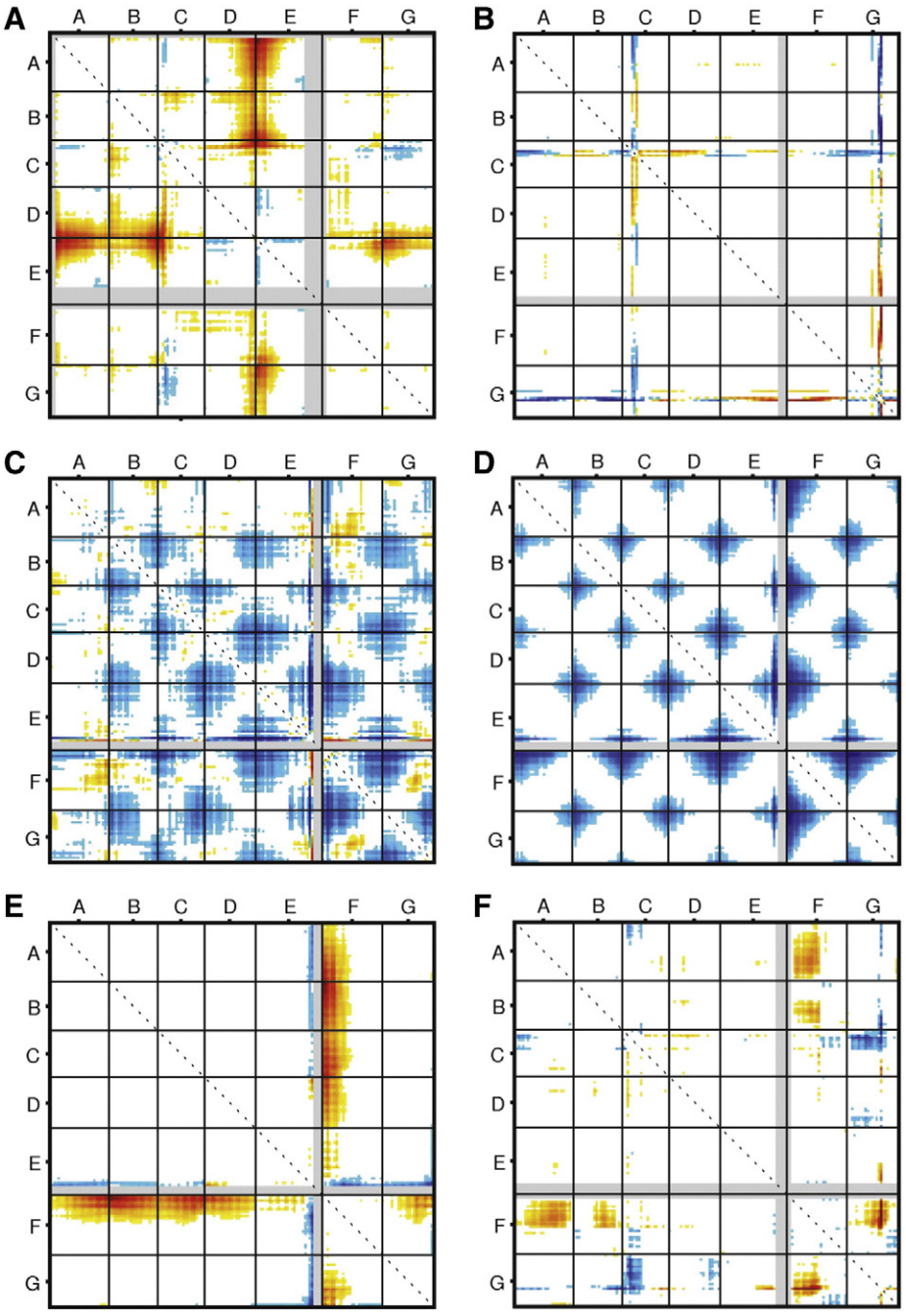

Fig. 4. Single value decomposition analysis of the major branches (containing two or more pdb entries) of the hierarchal tree shown in Fig. 3. The matrices show the principle component resulting from SVD analysis of the difference internal distance matrices from the following sets: A, 1JV6–1BRX (D85S/F219L mutant [21]), 1JV7–1BRX (D85S mutant [21]) and 1XOI–1IW6 (acid blue [75]). B, 1QKO–1QKP$_{gnd}$ (K-state [16]), 1QKP$_{exc}$–1QKP$_{gnd}$ (K-state [16]) and 1M0M$_{exc}$–1M0M$_{gnd}$ (M1-state [65]). C, 1O0A$_{exc}$–1O0A$_{gnd}$ (L-state [66]), 1P8H$_{exc}$–1P8H$_{gnd}$ (M1-state [67]) and 1P8U$_{exc}$–1P8U$_{gnd}$ (N-state [67]). D, 1C3W–1O0A$_{gnd}$ (two bR states, [33,66]). E, 1FBK–1FBB (D96G/F171C/F219L triple mutant [22]) and 4FPD–1KGB (D96G/F171C/F219L triple mutant [74]). F, 1F4Z–1F50 (M-state [20]), 2NTW–2NTU (L-state [69]), 2I20–2I1X (M-state [68]), 1CWQ$_{exc}$–1CWQ$_{gnd}$ (M-state [19]), 1KG8–1KGB (M-state [63]), 3VI0–3VHZ (O-state [73]), 1DZE–1IW6 (M-state [71]), 1IW9–1IW6 (M-state [71]), 2ZZL–1IW6 (M-state [72]), 1E0P–1QHJ (K:L:M with ratio 1:3:1 [18]) and 1VJM–1QHJ (L-state [62]). See Section 5 for a description of these clusters and their structural interpretation. Red indicates a reproducible movement of C_α atoms away from each other whereas blue indicates a reproducible movement towards each other.

all major groups to contribute to the field: Luecke (1F4Z–1F50) [20]; Lanyi (2NTW–2NTU) [69] and (2I20–2I1X) [68]; Büldt (1CWQ$_{exc}$–1CWQ$_{gnd}$); Glaeser (1KG8–1KGB) [63]; Kouyama (3VI0–3VHZ) [73], (1DZE–1IW6) [71], (1IW9–1IW6) [71] and (2ZZL–1IW6) [72]; and ourselves (1E0P–1QHJ) [18] and (1VJM–1QHJ) [62]. Moreover a twelfth structure (1C8S–1C8R) [17], which did not model large cytoplasmic regions of helices E and F, also lies adjacent to this cluster. *Thus this set of deposited pdb structures display light induced conformational changes that are consistent across many studies and are replicated by independent research groups using different crystal forms*. We therefore take the view that these conformational changes most likely represent what is happening in reality. This conclusion comes with the caveat that any motion within 3D crystals is constrained by the need to maintain sufficient crystalline order for diffraction to be recorded. An SVD analysis of this set of structures reveals that the major light induced conformational changes common to these eleven studies correspond to a movement of the extracellular portion of helix C towards helix G, and a movement of the cytoplasmic portions of helix F away from helices A,

B and G (Fig. 4F). These movements were already described fourteen years ago [18–20] and it is noteworthy that, when the Pearson correlation coefficient is calculated for each member of this set of eleven structures against the principle SVD component, it is the two oldest structures within this set (1E0P–1QHJ) [18] and ($1CWQ_{exc}$–$1CWQ_{gnd}$) [19] that are most strongly correlated with these reproducible structural changes, having PCC values of 0.88 and 0.87 respectively.

6. Difference Fourier analysis of light induced structural changes

In the analyses above we sorted the bR-wild type structures (Fig. 2) and structural changes (Fig. 3) in order to identify similarities and differences in the positions of C_α-atoms within all relevant pdb entries. Whereas this analysis extracts conserved global motions, it does not specifically describe local changes in the vicinity of the isomerized retinal. The appropriate method with which to observe local structural changes is difference Fourier analysis, whereby the following Fourier transform (FT) is made to recover the difference electron density:

$$\Delta\rho(\mathbf{x}) = \mathrm{FT}\left(\left({F_{exc}}^{obs} - {F_{gnd}}^{obs}\right) \cdot \exp\left(i\Phi_{gnd}\right)\right)$$

which simply presents the experimental changes in the X-ray diffraction data in real space using the resting state structural model for phases (Φ_{gnd}) [80]. The critical point is that the resulting difference electron density, $\Delta\rho(\mathbf{x})$, has no phase bias towards the intermediate state model since that model never enters the calculation. Difference Fourier analysis is not always possible since it requires that the two data sets are isomorphous and for highly twinned data it is not possible to extract F^{obs} without additional assumptions. Of the 19 crystallographic studies of light driven structural changes in bR (Table 2), crystallographic observations for eight of these are available in the protein data bank. From these data we have calculated Bayesian error weighted difference Fourier electron density maps [81] and these are presented in Fig. 5.

Three crystal structures of the bR K-intermediate have been described [16,57,64] and all trapped this early intermediate using green light illumination at 100 K or 110 K (Table 2). Crystallographic data were released for one of these studies [16] and the error weighted difference Fourier map (data-set C, 1QKP–1QHJ) is shown in Fig. 5A. The strongest feature of the entire difference electron density map is a negative peak on Wat402 that is visible to a confidence level of 9.1 σ (here we take σ to be the root mean square electron density within the unit cell and we quote values as displayed in Coot [82]) and indicates that Wat402 is disordered by retinal isomerisation. Consequently, when interpreting this feature we removed Wat402 from our K-state model. Other structural changes indicated by the difference density and captured by structural refinement include a weakening of the H-bond interaction from Thr89 to Oδ1 of Asp85 and a side-ways movement of the Lys216 side-chain (Fig. 5A). As noted above, all strong difference electron density features clustered around the retinal chromophore and we allowed only a few residues to move during structural refinement (Figs. 3; 4B).

Kouyama presented convincing difference electron density showing a movement of the Lys216 side-chain in K [57] but also observed that a negative difference density feature can arise on Wat402 due to radiation damage (see Section 7). In modeling this structural intermediate Kouyama went to some lengths to compensate for this effect [57] and Wat402 was retained in the K-state model. Lanyi retained both the position of Wat402 and the SB-Wat402 H-bond interaction in K [64]. Examining this pdb file (1M0K), however, shows a significant increase in the crystallographic B-factor of Wat402 in the K-state model (B = 39.9 Å^2) relative to the resting state (B = 24.5 Å^2) and this increase was not observed for the SB nitrogen nor Oδ1 and Oδ2 of Asp85. An increase in crystallographic B-factor implies that light-activation also induced some disordering of Wat402 in Lanyi's K-state study.

Five studies of the L-intermediate have been reported [18,62,66,69,70], which highlights the high functional importance placed on understanding this structural intermediate which sets the stage for the primary proton transfer event from the SB to Asp85 (Fig. 1). Crystallographic data were released for four of these studies [18,62,69,70] and error weighted difference Fourier maps calculated from these data are presented in Fig. 5B–E. The L-state of Kouyama [70] also shows a negative density peak on Wat402 (visible to 5.2 σ; Fig. 5B) but also has stronger features visible immediately towards the cytoplasmic side of the retinal than observed in K (Fig. 5A). Kouyama used green light illumination at 160 K followed by red light illumination at 100 K to trap this intermediate state (Table 2) and it would be expected that more structural relaxation is observed than when using green light illumination at 110 K.

All difference electron density maps calculated from three L-state studies using the LCP crystal form show a remarkable level of agreement (Fig. 5C–E). In our first study we illuminated crystals with green light for 40 s at 170 K, followed by 30 s relaxation prior to quenching in liquid nitrogen [18]. In addition to revealing a disordering Wat402 (visible to 7.2 σ) and movements of the side-chain and back-bone of Lys216 already seen in K, this difference density map (Fig. 5D) showed the disordering of two further water molecules within the channel (Wat400 and Wat401); the ordering of a new water molecule (Wat451) between Asp85 and Asp212; the breakage of the H-bond from Thr89 to Asp85; a movement of Trp182 towards the cytoplasm; and a reorientation of the side-chain of Arg82 towards the extracellular media (Fig. 5D; 1E0P–1QHJ). Most strikingly, the difference Fourier electron density map revealed paired positive and negative density features aligned along the extracellular portion of helix C, which we interpreted to show a light induced flex of the extracellular half of helix C towards helix G. As described in Section 5, this movement is observed (with varying levels of confidence) in 11 independent crystallographic studies of trapped intermediate states (Figs. 3, 4 F). Our trapping protocol was criticized at the time for not producing a pure spectral intermediate but rather a 1:3:1 mixture of the K, L and M [61]. We therefore repeated this study using red light illumination at 150 K for which the spectral evidence established a pure L-state [62]. The resulting difference Fourier electron density map (Fig. 5E) and refined crystallographic structure showed all structural changes previously reported using green light illumination at 170 K [18] including a negative density peak associated with Wat402 (visible to 5.0 σ).

Lanyi and colleagues first trapped the L-state by illuminating bR crystals with red light at 170 K [66]. Their analysis produced a structure of L which is slightly shortened relative to bR in a direction perpendicular to the membrane (Figs. 3; 4C, 1O0A). These authors later repeated this trapping protocol but modified it to collect both resting and illuminated state diffraction data from the same crystal [66]. Crystallographic data for the latter study were released and are of very high quality, producing the most convincing error weighted difference Fourier electron density map (2NTW–2NTU, Fig. 5C) of any study of illuminated crystals. A very strong negative difference density feature shows the disordering of Wat402 (visible to 19.0 σ). Movements of the Lys216 side-chain and backbone; the disordering of Wat400 and Wat401 and a corresponding ordering of Wat451 between Asp85 and Asp212; the breakage of the H-bond interaction from Thr89 to Asp85; the displacement of Trp182 towards the cytoplasm; the beginning of a movement of the side-chain of Arg82 towards the extracellular media; and paired negative and positive difference density features that align along the extracellular portion of helix C, indicating a flex of this helix towards helix G, are all indicated within this difference density map. We gladly acknowledge this high-quality crystallographic data from Lanyi and co-workers that convincingly demonstrates the same electron density changes in L [69] that we observed seven years earlier [18]. What puzzles us, however, is that few of these movements were actually modeled in the deposited L-state structure, apart from the sideways movement of Lys216 and a very subtle shift in C_α-positions in helix C (Fig. 5C, purple bR, red L).

Crystallographic studies of the trapped M-intermediate have been less controversial. Most M-state trapping studies applied a protocol of illuminating crystals during a short period of thawing as the cryo-stream was blocked and the crystal warmed to room temperature [17,19,20,67,68]; or alternatively illuminating bR crystals at 210 K or 230 K [63,65] (Table 2). For vesicle fusion crystals of bR the photocycle is slowed 100 fold and it was therefore possible to achieve high M-state occupancy when illuminating crystals at room temperature [71,72]. Ten pdb entries describe trapped M-states and, with one exception [65], all have modeled (to varying degrees) the same structural changes as described above: the disordering of Wat402, Wat400 and Wat401 and ordering of Wat451 between Asp85 and Asp212; the breakage of

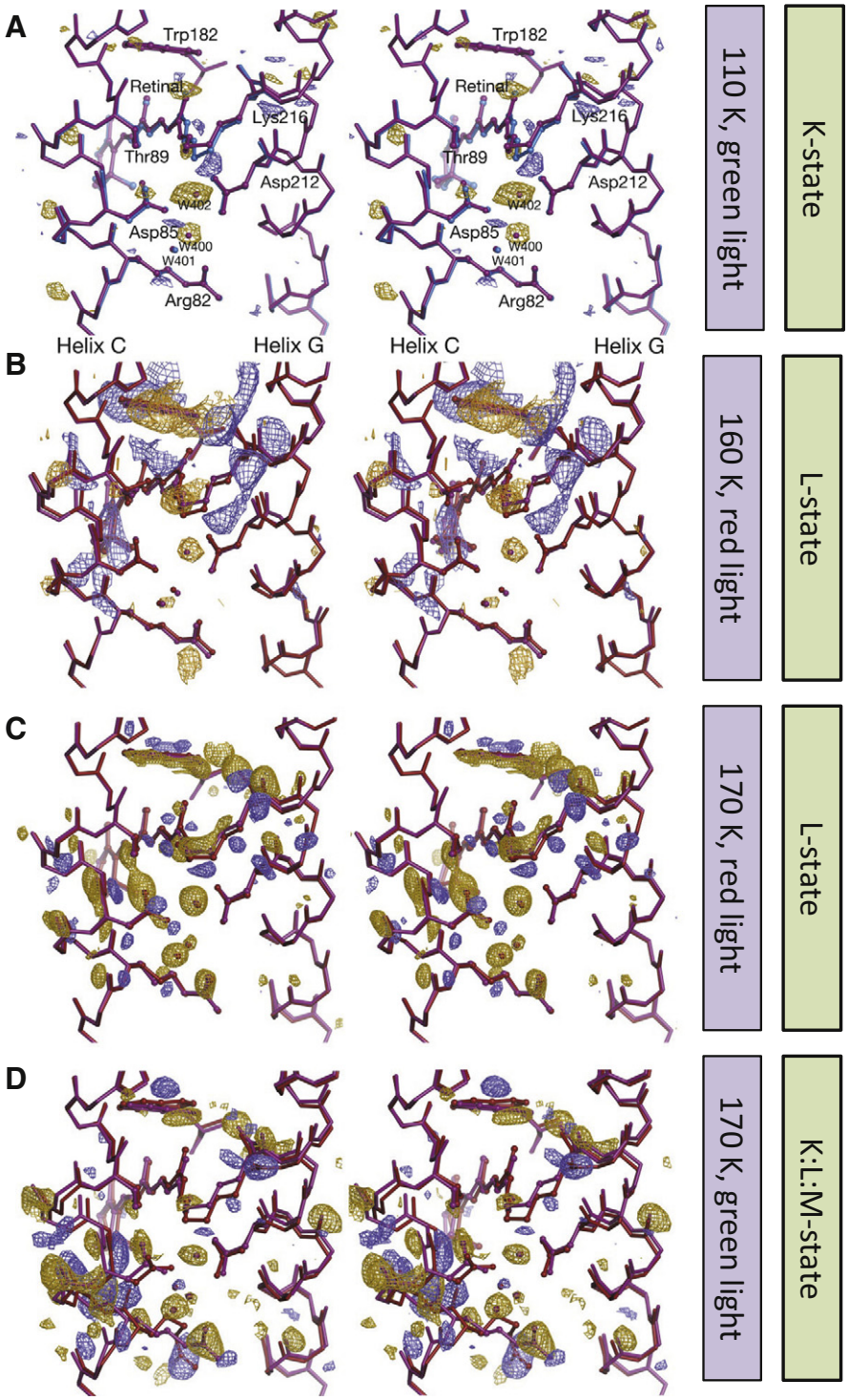

Fig. 5. Difference Fourier analysis of crystallographic data deposited from studies of light-induced structural changes in bR. A, A K-intermediate [16] (1QKP–1QHJ). B, An L-intermediate [70] (1UCQ–1IW6). C, An L-intermediate [69] (2NTW–2NTU). D, A 1:3:1 mixture of K:L:M [18] (1E0P–1QHJ). E, An L-intermediate [62] (1VJM–1QHJ). F, An M-intermediate [72] (2ZZL–1IW6). G, An M-intermediate (2I20–2I2X) [68]. H, An O-intermediate [73] (3VI0–3VHZ). Both the resting state bR structure (purple) and the corresponding intermediate state structure (Blue, K; red, L; yellow, M; pink, O) are also shown. Difference Fourier map CNS scripts that have been modified to take q-weighting into account were obtained from Thomas Ursby (MAX IV Laboratory, Lund, Sweden) and are provided as supplementary information [81]. Positive difference electron density is blue and negative difference electron density is yellow. All panels are contoured at different levels because varying quality from map to map. This figure is drawn in stereo.

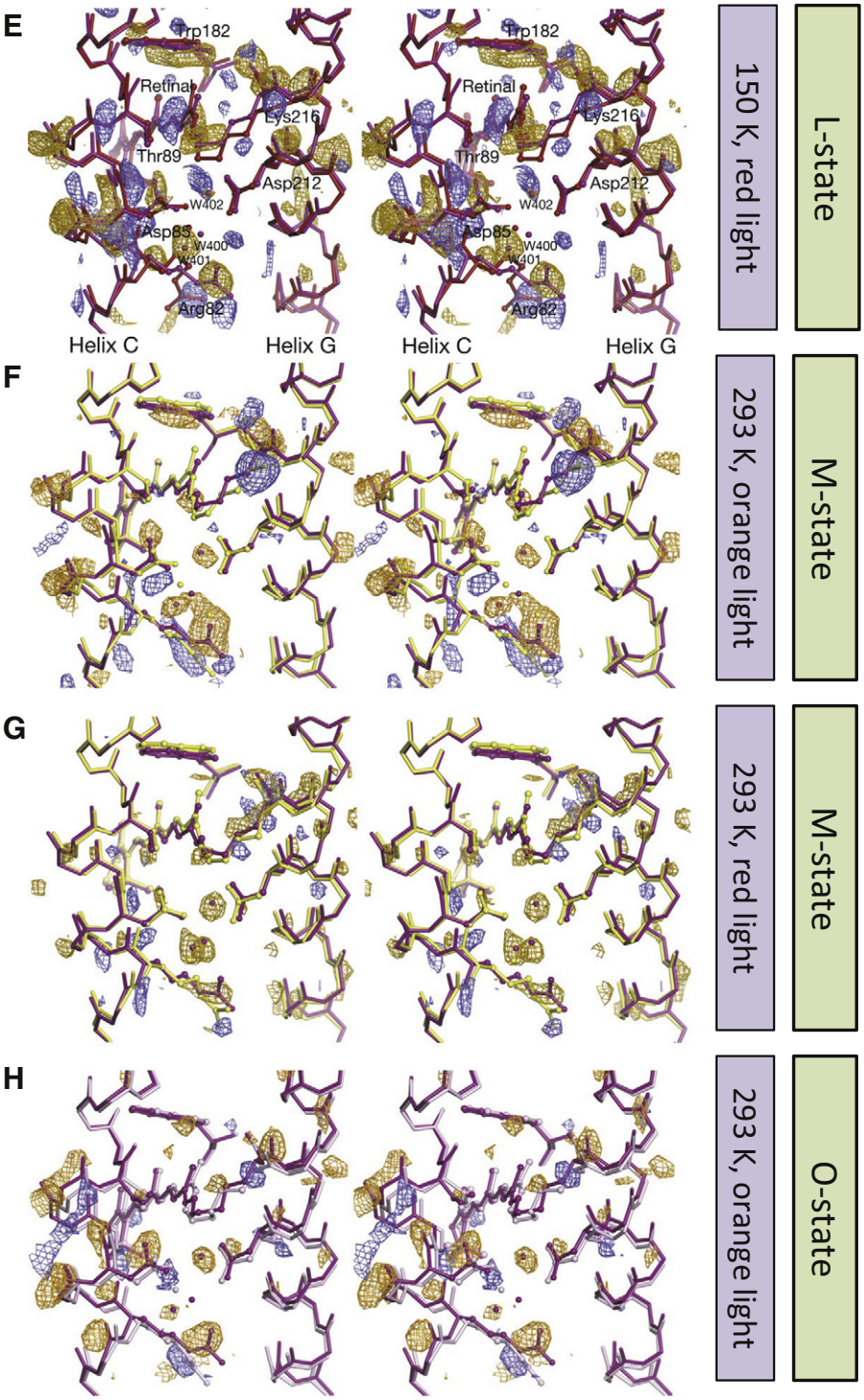

Fig. 5 (*continued*).

the H-bond interaction from Thr89 to Asp85; movements of both the Lys216 side-chain and backbone; a displacement of Trp182 towards the cytoplasm; and the reorientation of the side-chain of Arg82 towards the extracellular media [17,19,20,63,67,68,71]. Error weighted difference Fourier electron density maps calculated for the two M-state intermediates for which crystallographic data were deposited [68,72] support these conclusions since both show difference density features consistent with the modeled structural changes (2ZZL–1IW6, Fig. 5F; 2I20–2I1X, Fig. 5G). In particular, negative difference electron density on Wat402 is visible to 7.4 σ in the map calculated from Lanyi's M-state data (Fig. 5G), and to 5.6 σ in the map calculated from Kouyama's data (Fig. 5F). Indeed, many of the structural changes indicated in Lanyi's L-state difference density map (Fig. 5C) are also visible in his M-state difference density map (Fig. 5G) but structural refinement was more successful in capturing these motions in M (Fig. 5G, purple bR, yellow M).

Our sorting algorithm developed from a Pearson correlation analysis of C_α displacements placed seven of these ten M-state structures within the same branch of the hierarchal tree (Fig. 3, PCC ≥ 0.597) and an SVD analysis of the eleven structures within this cluster showed that they share movements of the extracellular portion of helix C towards helix

G and the cytoplasmic portion of helix F away from helices A, B and G (Fig. 4F). Apart from the first M-state of Luecke [17], which would be included within this branch if the threshold PCC ≥ 0.597 were relaxed, the remaining two M-state structures are from Lanyi: one of which (1PH8 [67]) shows the M-state to be compressed perpendicular to the membrane (Fig. 4C) and the other (1M0M, [65]) shows C_α movements two orders of magnitude smaller than observed for all other M-state structures ($S(1M0M_{exc}–1M0M_{gnd}) = 0.002$ Å, Fig. 3).

No diffraction data were deposited for the only trapped N-state structure [67], but Kouyama trapped an O-intermediate in the L93A bR mutant at room temperature [73] and released these crystallographic data. The error weighted difference Fourier electron density map calculated from these data (3VI0–3VHZ, Fig. 5H) is consistent with all the other difference density maps presented above (Fig. 5), showing a negative peak on Wat402 (visible to 4.7 σ) and paired difference density features associated with helix C that indicate a movement of the extracellular portion of this helix towards helix G. Moreover, structural refinement of the O-state successfully captured all conformational changes visible within this difference electron density and this structure clusters within the major branch of bR photo-intermediates (Fig. 3).

In summary, by examining the experimental changes in electron density represented using difference Fourier analysis we observe a high level of agreement (with varying levels of noise) from one study of light-induced structural changes in bR to another (Fig. 5). There is, naturally, considerable variation concerning the functional importance assigned to conformational changes reproducibly observed, as is the liberty of any author to interpret their own observations. Moreover, a number of studies emphasized structural features that have been less reproducible from one study to another, most notably the ordering of water molecules within the cytoplasmic portion of the channel [19,20,70,73,74]. In our view these considerations are absolutely reasonable, but we wish here to emphasize that the key ingredients required to understand the mechanism of proton pumping by bR [23] have been reproducibly observed by different groups in multiple independent studies.

7. X-ray induced radiation damage

Protein crystallography recovers structural information by placing a protein crystal in the path of an intense X-ray beam and recording diffraction patterns. For every X-ray photon scattered approximately ten are absorbed within the protein crystal and produce photo-electrons, which in turn induce secondary ionization events [83]. These liberated electrons cause damage and the influence of X-ray induced damage on protein structure has been extensively studied [84]. A number of clear trends have emerged and it is a general property that aspartic and glutamic acids are the most sensitive residues since exposure to X-ray can cause their carboxylic head group to be cleaved, even at cryogenic temperature [85]. Acidic residues near or within an enzyme's active site appear to be especially sensitive, as has been observed for lysozyme [86,87], acetylcholinesterase [86,87], myrosinase [88] maltooligosyltrehalose trehalohydrolase [89], trypsin [89], a photosynthetic reaction centre [90] and green fluorescent protein [91].

From these findings it might be expected that one or both of the active site aspartate residues of bR will become cleaved by X-ray induced damage. Kouyama was the first to investigate this issue and indeed observed that the head group of Asp85 is eventually cleaved by X-rays even at cryogenic temperature [57]. A later study of X-ray damage by Gordeliy drew similar conclusions [58]. In this case the crystallographic data were deposited and the error weighted difference Fourier electron density map is very convincing (Fig. 6B, 3NSB–3NS0). In particular, extremely clear negative difference density that covers the entire head group of Asp85 is visible to an exceptionally high confidence level (20.2 σ) and is the strongest feature of the map. Similarly, the head group of Asp212 is also covered by a strong negative density feature. Thus the head-groups of both active site aspartates are cleaved by exposure to X-rays and it cannot be any surprise that the water molecules to which they form H-bonds (Wat400, Wat401 and Wat402) also disorder.

At lower X-ray dose another species, termed the orange species since bR changes colour, is also known to build up. Kouyama concluded that the structural changes associated with this species were significantly less than those associated with the K-intermediate, and that the fraction of molecules thus affected could not perform the regular photocycle upon light activation [57]. Gordeliy and co-workers also carefully investigated the structure of the orange species [78] by minimizing the X-ray fluence through a bR crystal (PDB entries 4MD1 (orange species) and 4MD2 (ground state)). The resulting difference Fourier map (4MD1–4MD2, Fig. 6A) exhibits paired negative and positive peaks associated with the SB region of the chromophore and Wat402, suggesting their slight displacement. One scenario compatible with these observations is that the SB becomes deprotonated due to the build-up of radicals induced by hydrated electrons generated in the solvent region of the crystal. This results in the lengthening of the H-bond from the SB nitrogen to Wat402, which moves away by a few tenths of an Angstrom. A similar X-ray induced deprotonation of another Schiff base was observed in crystallographic studies of phosphoserine aminotransferase [92].

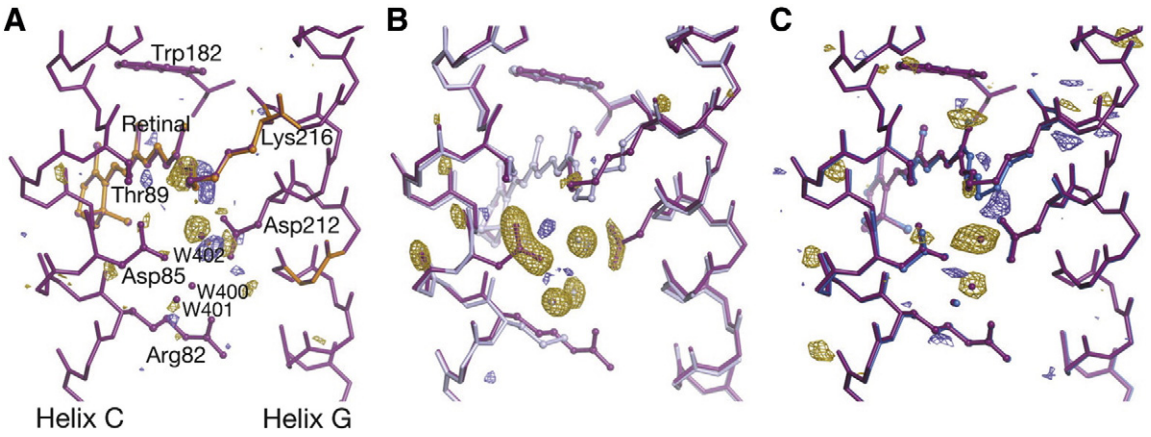

Fig. 6. Comparison of X-ray induced and light induced electron density changes at low-temperature. A, Difference Fourier electron density map recovered following low-dose X-ray induced build-up of the orange species at 100 K [78] (4MD1–4MD2). B, Difference Fourier electron density map recovered following higher dose X-ray induced radiation damage at 100 K [58] (3NSB–3NS0). C, Difference Fourier electron density recovered from light induced structural changes at 110 K [16] (1QKP–1QHJ). Positive difference electron density is blue and negative difference electron density is yellow.

These damage studies are based upon sound crystallographic work and warrant reconsideration of earlier intermediate trapping studies. As shown in Fig. 6B and C, both the K-state and radiation damage difference density maps show strong negative density features on Wat400 and Wat402. However, the K-state data (data-set C, 1QKP–1QHJ, [16]) has no negative density on Asp212 and only weak negative density on Oδ1 of Asp85 (Fig. 6C), a feature that is visible in almost all difference Fourier maps calculated for the light-driven studies of bR (Fig. 5). This is in contradistinction with the radiation damage map (Fig. 6B, 3NSB–3NS0), which shows negative density covering the entire head groups of both Asp85 and Asp212. Moreover, paired positive and negative difference density indicate a movement of the side-chain and backbone of Lys216 in K, but these positive density features are not visible in the high-dose radiation damage map. Finally, refined movements of C_α positions reveal structural changes due to low-dose and high-dose radiation damage that do not cluster with any other study of bR (Fig. 3; PCC $\leq$ 0.32 relative to all other studies). Of the difference Fourier maps calculated from the deposited data, only the L-state study from Lanyi [69] shows negative difference electron density extending from Oδ1 to Oδ2 of Asp85 (Fig. 5C). Even for this case, however, while some radiation damage cannot be ruled out it clearly makes only a minor contribution to the observed difference density. Admittedly, of the three K-state data sets that we deposited fifteen years ago, the other two (data-sets A and B in 1QKP) show indications of radiation damage on Asp85. We are thus again reminded of the benefits of making diffraction data available for posterity since, if the data are available, structural conclusions can be reconsidered in light of new ideas.

From these structural observations it appears that a similar mechanism operates in the two cases: when light-activates bR, retinal isomerization breaks the SB-Wat402 H-bond and disorders Wat402. When X-rays cleave the head groups of Asp85 and Asp212, this also breaks their H-bond interactions to Wat400, Wat401 and Wat402 and these water molecules disorder. These findings are completely consistent with one another and concerns that the light-induced disordering of Wat402 observed in the K-state was due to radiation damage [58] rather than retinal isomerization may have been overstated.

8. A unified view of structural changes in the bR photocycle

From the analysis presented in Section 5, in which we took a step back and quantitatively analysed global conformational changes of C_α atoms in all intermediate trapping and relevant mutation studies of bR, a number of strong conclusions can be drawn: (I) C_α movements associated with the low-temperature K-intermediate are small; (II) Reproducible movements of C_α atoms ($PCC_{ij} \geq 0.597$) are observed in eleven deposited pairs of pdb entries recovered from studies of light induced structural changes in bR, with the common motions being movements of the extracellular portion of helix C towards helix G, and a movement of the cytoplasmic portion of helix F away from helices A, B and G (Fig. 4F); (III) The D96G/F171C/F219L bR triple mutant displays a significant structural perturbation corresponding to movements of the cytoplasmic portion of helix F away from helices A, B, C, D, and G (Fig. 4E). These mutation induced changes are significantly larger than, yet correlate with, the reproducible structural changes induced by light. Solution state time-resolved X-ray scattering [93], time-resolved X-ray diffraction from 2D crystals [94], and X-ray [95,96], neutron [97] and electron [98] diffraction from 2D crystals with trapped bR intermediates, all indicate that the larger amplitude of the helix F movement observed in the triple mutant structure more accurately represents this motion in vivo, suggesting that the smaller movements seen in 3D crystals are constrained by the crystal lattice.

From these results we are led to a picture of global conformational changes in the bR photocycle which is considerably simpler than what it might first seem when entering the literature (Table 2). Instead of multiple competing motions, there is basically one type of motion primarily associated with helices C and F (Fig. 7, Supplementary Movie 1), although the extent to which the full light induced motions of helices E and F are best captured by intermediate trapping or mutational studies can be debated. A striking aspect of this consensus picture is that very similar conclusions were drawn from time resolved wide angle X-ray scattering (WAXS) data recorded for a sequence of time-delays from 360 ns to 100 ms following photo-activation of wild-type bR in solution [93]. Time resolved WAXS is an emerging method that is sensitive to global protein rearrangements [99–103]. In these studies, time-dependent changes in WAXS data throughout the bR photocycle were modeled by assuming an inwards motion of helix C, an outwards motion of helices E and F, and a rearrangement of helix G [93]. These movements grew with a half-rise of 22 μs, preceding the SB deprotonation as measured using transient changes in absorption at 410 nm; these motions increased in amplitude by half again after SB deprotonation with a half-rise of 1.9 ms; and this conformational change relaxed back to the resting bR conformation with a half-life of 16 ms. Thus experimental data using a completely different, time-dependent X-ray structural probe are in keeping with the major structural conclusions that emerged from our hierarchal sorting of the deposited pdb structures.

Our analysis of difference Fourier electron density maps calculated from the deposited crystallographic data also yield remarkably consistent conclusions. Most strikingly, all deposited crystallographic data show a strong negative difference density peak on Wat402, and this is usually one of the strongest features of the difference Fourier electron density map. Other reproducible features, but which vary in significance from map to map due to experimental noise, include negative density on Wat400 and Wat402 and a positive density feature interpreted as a newly ordered water (Wat451); negative and positive density indicating a sideways movement of the Lys216 side chain; a movement towards the cytoplasm of the side chain of Trp182; a negative density feature on Oδ1 of Asp85 which suggests a loss of its H-bond interaction with Thr89; paired negative and positive difference density suggesting a reorientation of the side-chain of Arg82 towards the extracellular medium; and paired difference density features that show a movement of the extracellular portion of helix C towards helix G. These difference density changes have been modeled by different groups as indicating similar changes in protein structure. Most controversy has therefore concerned the timing of specific structural changes, and in particular whether or not specific motions of water molecules or other residues should be assigned to the K, L, M1 or M2 intermediates, rather than the nature of the structural changes that arise in the bR photocycle.

9. How does bR pump protons up-hill against a transmembrane potential?

To a good approximation, proton pumping by bR can be thought of as being governed by two major conformations: the relaxed bR resting state with an all-*trans* retinal conformation and Wat402 forming H-bonds to the retinal-SB, Asp85 and Asp212 (Fig. 7); and a second conformation with the retinal in a 13-*cis* geometry and the SB-Wat402 H-bond broken (Supplementary Movie 1). In this configuration the SB points approximately towards the cytoplasm, Wat402 is displaced and the H-bond network maintaining the rigid structure of the extracellular portion of the protein has collapsed such that helix C moves closer to helix G and a physical force of the retinal on Trp182 of helix F has driven an outwards tilt of the cytoplasmic portion of this helix (Fig. 7).

In relating these structures to function it is critical to understand that in the bR resting state the pKa of the SB is 13.5 [104] and that of Asp85 is 2.2 [105]. Thus, even though a pathway exists for rapid proton exchange along a water mediated H-bond network connecting the SB and Asp85, *no net proton transfer occurs since natural selection long ago tuned the resting-state bR structure to ensure that the proton affinity of the SB is several orders of magnitude greater than that of Asp85.* Photo-isomerization of the all-*trans* retinal to its 13-*cis* conformation reorients

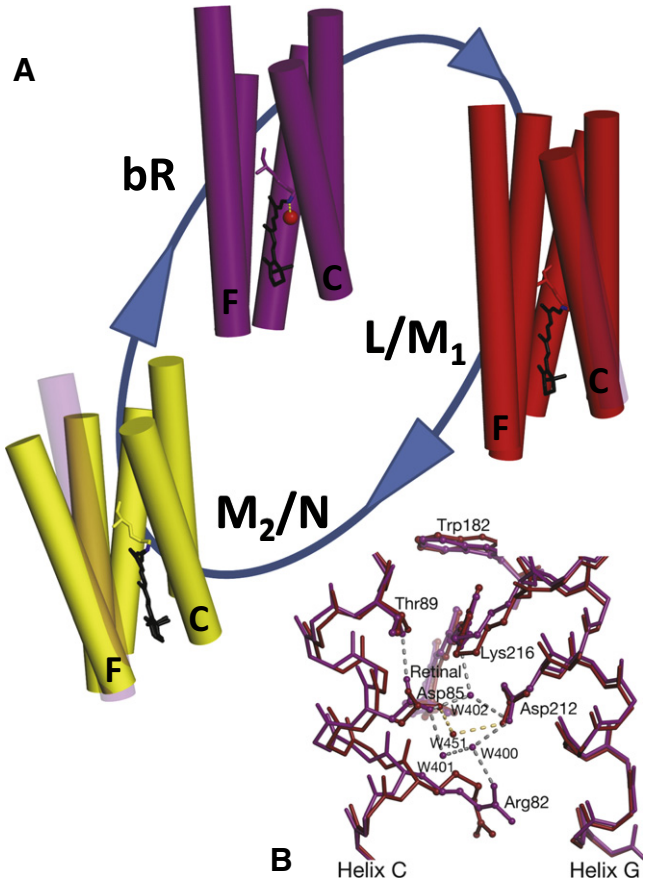

Fig. 7. Overview of structural changes in the bR photo-cycle. Two major conformations are sufficient to understanding the mechanism of proton pumping by bR. The resting bR state in which Wat402 forms H-bonds to the SB, Asp85 and Asp212; and the relaxed illuminated state in which these H-bonds are disrupted and helix C moves towards helix G. These conformational changes set the stage for proton transport from the SB to Asp85. Larger scale changes associated with helix F are needed to facilitate reprotonation of the retinal from the cytoplasm. To illustrate helix movements, the resting bR structure (purple) of helix C and helix F are overlaid on the intermediate state conformations (L/M1, red; M2/N, yellow) as transparent helices (purple). Helices A and B are removed from the figure for convenience.

the protonated SB into a hydrophobic pocket and breaks the H-bond connection to Wat402, a critical H-bond that stabilizes the elevated SB pKa [106]. Both structural perturbations therefore lower the SB pKa. As Wat402 disorders, Asp85 loses H-bond interactions to this water molecule and to Thr89 and its carboxylate group is forced closer to the negative charge of Asp212 as helix C bends towards helix G. These structural perturbations increase the pKa of Asp85 [18,62]. *By lowering the SB pKa and increasing that of Asp85, a point is eventually reached where the proton affinities of these two key functional groups are similar and a proton transfer becomes probable.* The precise moment when a proton is exchanged will not be governed by the average conformation caught using X-ray crystallography, but instead will depend upon fluctuations about the average structure that transiently connect the SB to Asp85 [62,107,108]. Because the mutual electrostatic attraction between the positively charged SB and the negatively charged Asp85 is canceled when both chemical groups are neutralized by proton transfer, the driving force that draws these two groups together is lost and their connectivity is thereby broken [18,62]. A complementary effect was suggested by Subramaniam and Henderson who compared small molecule crystal structures of retinal and observed that the degree of retinal curvature is decreased in the deprotonated state [22]. Thus a putative straightening could pull the SB up to 0.7 Å away from Asp85 and also contribute to breaking the SB connectivity to the extracellular half-channel.

We previously argued that helix C might straighten after proton exchange and thereby pull Asp85 away from the SB so as to prevent the futile exchange of a proton from Asp85 to the SB [18,23,62]. The structural evidence presented here, however, requires that this idea be abandoned since the later intermediate states also cluster within the same branch of the hierarchal tree as our L-state structures, and therefore the observed movement of helix C cannot directly depend upon the SB and Asp85 being charged. Rather, it appears that helix C moves towards helix G in response to the disruption of water mediated H-bonds on the extracellular side of the protein, a disordering initiated by the photo-isomerization of the retinal that first disorders Wat402, and then other waters in a manner analogous to how dominos are knocked over in turn. Alternatively, one can appreciate that when the retinal has an all-*trans* configuration, the position of Wat402 defines an extended network of H-bonds that rigidly holds helix C and G apart [26]; whereas when light photo-isomerizes the retinal this keystone water molecule is kicked out and this rigid structure collapses towards a more relaxed protein configuration.

Lanyi has proposed a very different model for how bR functions as a proton pump, arguing that the H-bonds connecting Wat402 to the SB, Asp85 and Asp212 are not broken prior to proton transfer, but instead these interactions are maintained in the L-state [66,69]. In this picture a sequence of subtle bends and twists of the retinal, first one way and then another [66], are needed to understand the mechanism of light driven proton pumping. A key question that this mechanism raises is why a water mediated H-bond network in L [69] that is identical to that of the resting bR state, facilitates proton transfer from the SB to Asp85 in the L-to-M transition but prevents this in the resting state? Lanyi's mechanism is founded upon a sequence of nine structures of trapped intermediate states, of which three cluster within the main branch of light driven conformational changes (Fig. 3). Crystallographic data were deposited for two of these nine structures and both difference Fourier electron density maps calculated from these data show strong negative peaks on Wat402 (Fig. 5C, G): this negative peak has a significance of 7.4 σ in the M-state (2I20–2I1X) and a significance of 19.0 σ for the L-state (2NTW–2NTU). To comply with the above proton-pumping mechanism, Lanyi interprets these data to show that the SB-Wat402 H-bond is maintained in L but broken in M. In our view, the only consistent interpretation of these data is that Wat402 is disordered and the SB-Wat402 H-bond is broken in both.

10. Conclusion

There exists a considerable body of structural data concerning light and mutation induced structural changes in bR (Table 2) that is structurally rich and functionally relevant. In this review we have sought to take a step back and to view all the deposited crystallographic structures and crystallographic observations as a single set. Independent studies from independent groups have reproducibly observed similar conformational changes, both within the experimental difference electron density calculated from deposited data (Fig. 5) and within the deposited pdb files (Fig. 3). Our take-home message is that the structural mechanism of proton pumping by bR can be understood from these data and the key ingredients are not that complex: light driven retinal isomerization disrupts the keystone water molecule which connects the SB, Asp85 and Asp212 in the bR resting state; this disruption triggers a sequence of conformational changes (Supplementary Movie 1) that lower the pKa of the SB, increase the pKa of Asp85, and ultimately facilitates unidirectional proton transfer from the SB to Asp85. The connectivity between the SB and Asp85 is broken after proton transfer due to the neutralization of the attractive electrostatic force that draws these oppositely charged groups together [18] and a possible straightening of the retinal in its deprotonated state [22].

The primary proton transfer event and consequent breakage of the SB-Asp85 connectivity are the critical steps in achieving proton pumping uphill against a concentration gradient. Once achieved, the

remainder follows. This picture oversimplifies the mechanism of proton pumping so as to highlight its essence and therefore does not pay full credit to all chemically relevant conformational changes that have been observed by many authors. These include an outward movement of helix F, which allows water molecules to transiently order in the cytoplasmic half of the channel and thereby influence SB reprotonation from Asp96, and other structural factors that help control proton release to the extracellular medium. Despite this simplification it's important to appreciate that only the removal of the retinal chromophore or the mutation of Asp85 completely stops proton pumping by bR [109]. Even the D96G/F171C/F219L triple mutant, which is constitutively open, can pump protons with a high degree of efficiency without any large-scale conformational change [110].

Crystal structures of other light driven proton pumps such as xanthorhodopsin (XR) [111] and an unusual proteorhodopsin (ESR) [112] contain different extracellular proton release groups, have a histidine residue associated with their active sites, and ESR has a basic rather than acidic residue that serves as a cytoplasmic donor to the SB [112]. Despite these differences, XR, ESR, archaerhodopsin (AR) [113] and sensory rhodopsin II [114] (which pumps protons when not bound to its transducer [115]) all have a water molecule that accepts a H-bond from the SB and donates H-bonds to the carboxylate residues corresponding to Asp85 and Asp212. These observations strongly support the role of Wat402 as a functional keystone that is conserved in the mechanism of bacterial rhodopsin mediated phototrophy throughout the worlds' oceans.

Supplementary data to this article can be found online at http://dx.doi.org/10.1016/j.bbagen.2014.05.021.

Acknowledgments

We thank Thomas Ursby for providing scripts for calculating the q-weighted difference Fourier maps presented in Fig. 5. We thank Tsutomu Kouyama for providing crystallographic observations associated with the wild-type bR pdb entry 1IW6. We thank Valentin Borshchevskiy for allowing access to structures and experimental data corresponding to entries 4MD1 and 4MD2 prior to their release by the Protein Data Bank. We thank Frieda Reichsman for assistance in making Supplementary Movie 1. Financial support from the Knut and Alice Wallenberg Foundation (KAW), the Swedish Strategic Research Foundation (SSF), the Swedish Research Council (VR), the European commission Marie Curie Training Network NanoMem, and from the French National Research Agency (Grant ANR-11-JSV5-0009-01) is gratefully acknowledged.

References

[1] D. Oesterhelt, W. Stoeckenius, Rhodopsin-like protein from the purple membrane of Halobacterium halobium, Nat. New Biol. 233 (1971) 149–152.
[2] L.P. Kayushin, V.P. Skulachev, Bacteriorhodopsin as an electrogenic proton pump: reconstitution of bacteriorhodopsin proteoliposomes generating delta psi and delta pH, FEBS Lett. 39 (1974) 39–42.
[3] D. Oesterhelt, W. Stoeckenius, Functions of a new photoreceptor membrane, Proc. Natl. Acad. Sci. U. S. A. 70 (1973) 2853–2857.
[4] E.V. Lindley, R.E. MacDonald, A second mechanism for sodium extrusion in Halobacterium halobium: a light-driven sodium pump, Biochem. Biophys. Res. Commun. 88 (1979) 491–499.
[5] B. Schobert, J.K. Lanyi, Halorhodopsin is a light-driven chloride pump, J. Biol. Chem. 257 (1982) 10306–10313.
[6] J.L. Spudich, R.A. Bogomolni, Mechanism of colour discrimination by a bacterial sensory rhodopsin, Nature 312 (1984) 509–513.
[7] O. Beja, L. Aravind, E.V. Koonin, M.T. Suzuki, A. Hadd, L.P. Nguyen, S.B. Jovanovich, C.M. Gates, R.A. Feldman, J.L. Spudich, E.N. Spudich, E.F. DeLong, Bacterial rhodopsin: evidence for a new type of phototrophy in the sea, Science 289 (2000) 1902–1906.
[8] O.M. Finkel, O. Beja, S. Belkin, Global abundance of microbial rhodopsins, ISME J. 7 (2013) 448–451.
[9] U. Haupts, J. Tittor, D. Oesterhelt, Closing in on bacteriorhodopsin: progress in understanding the molecule, Annu. Rev. Biophys. Biomol. Struct. 28 (1999) 367–399.
[10] J.K. Lanyi, Mechanism of ion transport across membranes. Bacteriorhodopsin as a prototype for proton pumps, J. Biol. Chem. 272 (1997) 31209–31212.
[11] P. Brzezinski, R.B. Gennis, Cytochrome c oxidase: exciting progress and remaining mysteries, J. Bioenerg. Biomembr. 40 (2008) 521–531.
[12] J.E. Walker, The ATP synthase: the understood, the uncertain and the unknown, Biochem. Soc. Trans. 41 (2013) 1–16.
[13] M. Saidijam, K.E. Bettaney, G. Szakonyi, G. Psakis, K. Shibayama, S. Suzuki, J.L. Clough, V. Blessie, A. Abu-Bakr, S. Baumberg, J. Meuller, C.K. Hoyle, S.L. Palmer, P. Butaye, K. Walravens, S.G. Patching, J. O'Reilly, N.G. Rutherford, R.M. Bill, D.I. Roper, M.K. Phillips-Jones, P.J. Henderson, Active membrane transport and receptor proteins from bacteria, Biochem. Soc. Trans. 33 (2005) 867–872.
[14] R. Henderson, P.N. Unwin, Three-dimensional model of purple membrane obtained by electron microscopy, Nature 257 (1975) 28–32.
[15] R. Henderson, J.M. Baldwin, T.A. Ceska, F. Zemlin, E. Beckmann, K.H. Downing, Model for the structure of bacteriorhodopsin based on high-resolution electron cryo-microscopy, J. Mol. Biol. 213 (1990) 899–929.
[16] K. Edman, P. Nollert, A. Royant, H. Belrhali, E. Pebay-Peyroula, J. Hajdu, R. Neutze, E. M. Landau, High-resolution X-ray structure of an early intermediate in the bacteriorhodopsin photocycle, Nature 401 (1999) 822–826.
[17] H. Luecke, B. Schobert, H.T. Richter, J.P. Cartailler, J.K. Lanyi, Structural changes in bacteriorhodopsin during ion transport at 2 angstrom resolution, Science 286 (1999) 255–261.
[18] A. Royant, K. Edman, T. Ursby, E. Pebay-Peyroula, E.M. Landau, R. Neutze, Helix deformation is coupled to vectorial proton transport in the photocycle of bacteriorhodopsin, Nature 406 (2000) 645–648.
[19] H.J. Sass, G. Buldt, R. Gessenich, D. Hehn, D. Neff, R. Schlesinger, J. Berendzen, P. Ormos, Structural alterations for proton translocation in the M state of wild-type bacteriorhodopsin, Nature 406 (2000) 649–653.
[20] H. Luecke, B. Schobert, J.P. Cartailler, H.T. Richter, A. Rosengarth, R. Needleman, J.K. Lanyi, Coupling photoisomerization of retinal to directional transport in bacteriorhodopsin, J. Mol. Biol. 300 (2000) 1237–1255.
[21] S. Rouhani, J.P. Cartailler, M.T. Facciotti, P. Walian, R. Needleman, J.K. Lanyi, R.M. Glaeser, H. Luecke, Crystal structure of the D85S mutant of bacteriorhodopsin: model of an O-like photocycle intermediate, J. Mol. Biol. 313 (2001) 615–628.
[22] S. Subramaniam, R. Henderson, Molecular mechanism of vectorial proton translocation by bacteriorhodopsin, Nature 406 (2000) 653–657.
[23] R. Neutze, E. Pebay-Peyroula, K. Edman, A. Royant, J. Navarro, E.M. Landau, Bacteriorhodopsin: a high-resolution structural view of vectorial proton transport, Biochim. Biophys. Acta 1565 (2002) 144–167.
[24] W. Stoeckenius, Bacterial rhodopsins: evolution of a mechanistic model for the ion pumps, Protein Sci. 8 (1999) 447–459.
[25] T.R. Schneider, Objective comparison of protein structures: error-scaled difference distance matrices, Acta D Biol. Crystallogr. 56 (2000) 714–721.
[26] H. Belrhali, P. Nollert, A. Royant, C. Menzel, J.P. Rosenbusch, E.M. Landau, E. Pebay-Peyroula, Protein, lipid and water organization in bacteriorhodopsin crystals: a molecular view of the purple membrane at 1.9 A resolution, Structure 7 (1999) 909–917.
[27] Y. Kimura, D.G. Vassylyev, A. Miyazawa, A. Kidera, M. Matsushima, K. Mitsuoka, K. Murata, T. Hirai, Y. Fujiyoshi, Surface of bacteriorhodopsin revealed by high-resolution electron crystallography, Nature 389 (1997) 206–211.
[28] H. Michel, D. Oesterhelt, Three-dimensional crystals of membrane proteins: bacteriorhodopsin, Proc. Natl. Acad. Sci. U. S. A. 77 (1980) 1283–1285.
[29] E.M. Landau, J.P. Rosenbusch, Lipidic cubic phases: a novel concept for the crystallization of membrane proteins, Proc. Natl. Acad. Sci. U. S. A. 93 (1996) 14532–14535.
[30] E. Pebay-Peyroula, G. Rummel, J.P. Rosenbusch, E.M. Landau, X-ray structure of bacteriorhodopsin at 2.5 angstroms from microcrystals grown in lipidic cubic phases, Science 277 (1997) 1676–1681.
[31] J.L. Smith, R.F. Fischetti, M. Yamamoto, Micro-crystallography comes of age, Curr. Opin. Struct. Biol. 22 (2012) 602–612.
[32] H. Luecke, H.T. Richter, J.K. Lanyi, Proton transfer pathways in bacteriorhodopsin at 2.3 angstrom resolution, Science 280 (1998) 1934–1937.
[33] H. Luecke, B. Schobert, H.T. Richter, J.P. Cartailler, J.K. Lanyi, Structure of bacteriorhodopsin at 1.55 A resolution, J. Mol. Biol. 291 (1999) 899–911.
[34] V. Borshchevskiy, R. Efremov, E. Moiseeva, G. Buldt, V. Gordeliy, Overcoming merohedral twinning in crystals of bacteriorhodopsin grown in lipidic mesophase, Acta Crystallogr. D Biol. Crystallogr. 66 (2010) 26–32.
[35] L.C. Johansson, A.B. Wohri, G. Katona, S. Engstrom, R. Neutze, Membrane protein crystallization from lipidic phases, Curr. Opin. Struct. Biol. 19 (2009) 372–378.
[36] M. Caffrey, Crystallizing membrane proteins for structure determination: use of lipidic mesophases, Annu. Rev. Biophys. 38 (2009) 29–51.
[37] V. Cherezov, D.M. Rosenbaum, M.A. Hanson, S.G. Rasmussen, F.S. Thian, T.S. Kobilka, H.J. Choi, P. Kuhn, W.I. Weis, B.K. Kobilka, R.C. Stevens, High-resolution crystal structure of an engineered human beta2-adrenergic G protein-coupled receptor, Science 318 (2007) 1258–1265.
[38] D.M. Rosenbaum, V. Cherezov, M.A. Hanson, S.G. Rasmussen, F.S. Thian, T.S. Kobilka, H.J. Choi, X.J. Yao, W.I. Weis, R.C. Stevens, B.K. Kobilka, GPCR engineering yields high-resolution structural insights into β_2-adrenergic receptor function, Science 318 (2007) 1266–1273.
[39] D.M. Rosenbaum, S.G. Rasmussen, B.K. Kobilka, The structure and function of G-protein-coupled receptors, Nature 459 (2009) 356–363.
[40] L. Essen, R. Siegert, W.D. Lehmann, D. Oesterhelt, Lipid patches in membrane protein oligomers: crystal structure of the bacteriorhodopsin-lipid complex, Proc. Natl. Acad. Sci. U. S. A. 95 (1998) 11673–11678.
[41] K. Takeda, H. Sato, T. Hino, M. Kono, K. Fukuda, I. Sakurai, T. Okada, T. Kouyama, A novel three-dimensional crystal of bacteriorhodopsin obtained by successive fusion of the vesicular assemblies, J. Mol. Biol. 283 (1998) 463–474.

[42] S. Faham, J.U. Bowie, Bicelle crystallization: a new method for crystallizing membrane proteins yields a monomeric bacteriorhodopsin structure, J. Mol. Biol. 316 (2002) 1–6.
[43] S. Faham, G.L. Boulting, E.A. Massey, S. Yohannan, D. Yang, J.U. Bowie, Crystallization of bacteriorhodopsin from bicelle formulations at room temperature, Protein Sci. 14 (2005) 836–840.
[44] R. Ujwal, D. Cascio, J.P. Colletier, S. Faham, J. Zhang, L. Toro, P. Ping, J. Abramson, The crystal structure of mouse VDAC1 at 2.3 A resolution reveals mechanistic insights into metabolite gating, Proc. Natl. Acad. Sci. U. S. A. 105 (2008) 17742–17747.
[45] S.G. Rasmussen, H.J. Choi, D.M. Rosenbaum, T.S. Kobilka, F.S. Thian, P.C. Edwards, M. Burghammer, V.R. Ratnala, R. Sanishvili, R.F. Fischetti, G.F. Schertler, W.I. Weis, B.K. Kobilka, Crystal structure of the human beta2 adrenergic G-protein-coupled receptor, Nature 450 (2007) 383–387.
[46] H. Patzelt, B. Simon, A. terLaak, B. Kessler, R. Kuhne, P. Schmieder, D. Oesterhelt, H. Oschkinat, The structures of the active center in dark-adapted bacteriorhodopsin by solution-state NMR spectroscopy, Proc. Natl. Acad. Sci. U. S. A. 99 (2002) 9765–9770.
[47] M. Katragadda, J.L. Alderfer, P.L. Yeagle, Assembly of a polytopic membrane protein structure from the solution structures of overlapping peptide fragments of bacteriorhodopsin, Biophys. J. 81 (2001) 1029–1036.
[48] MATLAB, http://www.mathworks.se/products/matlab/ .
[49] N. Grigorieff, T.A. Ceska, K.H. Downing, J.M. Baldwin, R. Henderson, Electron-crystallographic refinement of the structure of bacteriorhodopsin, J. Mol. Biol. 259 (1996) 393–421.
[50] K. Mitsuoka, T. Hirai, K. Murata, A. Miyazawa, A. Kidera, Y. Kimura, Y. Fujiyoshi, The structure of bacteriorhodopsin at 3.0 A resolution based on electron crystallography: implication of the charge distribution, J. Mol. Biol. 286 (1999) 861–882.
[51] U.K. Genick, S.M. Soltis, P. Kuhn, I.L. Canestrelli, E.D. Getzoff, Structure at 0.85 A resolution of an early protein photocycle intermediate, Nature 392 (1998) 206–209.
[52] L.O. Essen, D. Oesterhelt, A cold break for photoreceptors, Nature 392 (1998) 131–133.
[53] W. Kuhlbrandt, Bacteriorhodopsin—the movie, Nature 406 (2000) 569–570.
[54] S. Subramaniam, M. Lindahl, P. Bullough, A.R. Faruqi, J. Tittor, D. Oesterhelt, L. Brown, J. Lanyi, R. Henderson, Protein conformational changes in the bacteriorhodopsin photocycle, J. Mol. Biol. 287 (1999) 145–161.
[55] S. Subramaniam, R. Henderson, Electron crystallography of bacteriorhodopsin with millisecond time resolution, J. Struct. Biol. 128 (1999) 19–25.
[56] T.O. Yeates, Detecting and overcoming crystal twinning, Methods Enzymol. 276 (1997) 344–358.
[57] Y. Matsui, K. Sakai, M. Murakami, Y. Shiro, S. Adachi, H. Okumura, T. Kouyama, Specific damage induced by X-ray radiation and structural changes in the primary photoreaction of bacteriorhodopsin, J. Mol. Biol. 324 (2002) 469–481.
[58] V.I. Borshchevskiy, E.S. Round, A.N. Popov, G. Buldt, V.I. Gordeliy, X-ray-radiation-induced changes in bacteriorhodopsin structure, J. Mol. Biol. 409 (2011) 813–825.
[59] J.K. Lanyi, H. Luecke, Bacteriorhodopsin, Curr. Opin. Struct. Biol. 11 (2001) 415–419.
[60] S.P. Balashov, T.G. Ebrey, Trapping and spectroscopic identification of the photointermediates of bacteriorhodopsin at low temperatures, Photochem. Photobiol. 73 (2001) 453–462.
[61] A. Royant, K. Edman, T. Ursby, E. Pebay-Peyroula, E.M. Landau, R. Neutze, Spectroscopic characterization of bacteriorhodopsin's L-intermediate in 3D crystals cooled to 170 K, Photochem. Photobiol. 74 (2001) 794–804.
[62] K. Edman, A. Royant, G. Larsson, F. Jacobson, T. Taylor, D. van der Spoel, E.M. Landau, E. Pebay-Peyroula, R. Neutze, Deformation of helix C in the low temperature L-intermediate of bacteriorhodopsin, J. Biol. Chem. 279 (2004) 2147–2158.
[63] M.T. Facciotti, S. Rouhani, F.T. Burkard, F.M. Betancourt, K.H. Downing, R.B. Rose, G. McDermott, R.M. Glaeser, Structure of an early intermediate in the M-state phase of the bacteriorhodopsin photocycle, Biophys. J. 81 (2001) 3442–3455.
[64] B. Schobert, J. Cupp-Vickery, V. Hornak, S. Smith, J. Lanyi, Crystallographic structure of the K intermediate of bacteriorhodopsin: conservation of free energy after photoisomerization of the retinal, J. Mol. Biol. 321 (2002) 715–726.
[65] J. Lanyi, B. Schobert, Crystallographic structure of the retinal and the protein after deprotonation of the Schiff base: the switch in the bacteriorhodopsin photocycle, J. Mol. Biol. 321 (2002) 727–737.
[66] J.K. Lanyi, B. Schobert, Mechanism of proton transport in bacteriorhodopsin from crystallographic structures of the K, L, M1, M2, and M2′ intermediates of the photocycle, J. Mol. Biol. 328 (2003) 439–450.
[67] B. Schobert, L.S. Brown, J.K. Lanyi, Crystallographic structures of the M and N intermediates of bacteriorhodopsin: assembly of a hydrogen-bonded chain of water molecules between Asp-96 and the retinal Schiff base, J. Mol. Biol. 330 (2003) 553–570.
[68] J.K. Lanyi, B. Schobert, Propagating structural perturbation inside bacteriorhodopsin: crystal structures of the M state and the D96A and T46V mutants, Biochemistry 45 (2006) 12003–12010.
[69] J.K. Lanyi, B. Schobert, Structural changes in the L photointermediate of bacteriorhodopsin, J. Mol. Biol. 365 (2007) 1379–1392.
[70] T. Kouyama, T. Nishikawa, T. Tokuhisa, H. Okumura, Crystal structure of the L intermediate of bacteriorhodopsin: evidence for vertical translocation of a water molecule during the proton pumping cycle, J. Mol. Biol. 335 (2004) 531–546.
[71] K. Takeda, Y. Matsui, N. Kamiya, S. Adachi, H. Okumura, T. Kouyama, Crystal structure of the M intermediate of bacteriorhodopsin: allosteric structural changes mediated by sliding movement of a transmembrane helix, J. Mol. Biol. 341 (2004) 1023–1037.
[72] M. Yamamoto, N. Hayakawa, M. Murakami, T. Kouyama, Crystal structures of different substrates of bacteriorhodopsin's M intermediate at various pH levels, J. Mol. Biol. 393 (2009) 559–573.
[73] J. Zhang, Y. Yamazaki, M. Hikake, M. Murakami, K. Ihara, T. Kouyama, Crystal structure of the O intermediate of the Leu93– > Ala mutant of bacteriorhodopsin, Proteins 80 (2012) 2384–2396.
[74] T. Wang, A.O. Sessions, C.S. Lunde, S. Rouhani, R.M. Glaeser, Y. Duan, M.T. Facciotti, Deprotonation of D96 in bacteriorhodopsin opens the proton uptake pathway, Structure 21 (2013) 290–297.
[75] H. Okumura, M. Murakami, T. Kouyama, Crystal structures of acid blue and alkaline purple forms of bacteriorhodopsin, J. Mol. Biol. 351 (2005) 481–495.
[76] N. Hayakawa, T. Kasahara, D. Hasegawa, K. Yoshimura, M. Murakami, T. Kouyama, Effect of xenon binding to a hydrophobic cavity on the proton pumping cycle in bacteriorhodopsin, J. Mol. Biol. 384 (2008) 812–823.
[77] T. Nishikawa, M. Murakami, T. Kouyama, Crystal structure of the 13-cis isomer of bacteriorhodopsin in the dark-adapted state, J. Mol. Biol. 352 (2005) 319–328.
[78] V. Borshchevskiy, E. Round, I. Erofeev, M. Weik, A. Ishchenko, I. Gushchin, A. Mishin, D. Willbold, G. Büldt, V. Gordeliy, Low dose X-ray radiation induces structural alterations in proteins, Acta Crystallogr. D Biol. Crystallogr. (2014) (in press).
[79] G. Zaccai, How soft is a protein? A protein dynamics force constant measured by neutron scattering, Science 288 (2000) 1604–1607.
[80] R. Henderson, J.K. Moffat, The difference Fourier technique in protein crystallography: errors and their treatment, Acta Crystallogr. B 27 (1971) 1414–1420.
[81] T. Ursby, D. Bourgeois, Improved estimation of structure-factor difference amplitudes from poorly accurate data, Acta Crystallogr. A 53 (1997) 564–575.
[82] Coot, http://www2.mrc-lmb.cam.ac.uk/Personal/pemsley/coot/ .
[83] R. Henderson, The potential and limitations of neutrons, electrons and X-rays for atomic resolution microscopy of unstained biological molecules, Q. Rev. Biophys. 28 (1995) 171–193.
[84] R.L. Owen, E. Rudino-Pinera, E.F. Garman, Experimental determination of the radiation dose limit for cryocooled protein crystals, Proc. Natl. Acad. Sci. U. S. A. 103 (2006) 4912–4917.
[85] E. Fioravanti, F.M. Vellieux, P. Amara, D. Madern, M. Weik, Specific radiation damage to acidic residues and its relation to their chemical and structural environment, J. Synchrotron Radiat. 14 (2007) 84–91.
[86] M. Weik, R.B. Ravelli, G. Kryger, S. McSweeney, M.L. Raves, M. Harel, P. Gros, I. Silman, J. Kroon, J.L. Sussman, Specific chemical and structural damage to proteins produced by synchrotron radiation, Proc. Natl. Acad. Sci. U. S. A. 97 (2000) 623–628.
[87] R.B. Ravelli, S.M. McSweeney, The 'fingerprint' that X-rays can leave on structures, Structure 8 (2000) 315–328.
[88] W.P. Burmeister, Structural changes in a cryo-cooled protein crystal owing to radiation damage, Acta Crystallogr. D Biol. Crystallogr. 56 (2000) 328–341.
[89] H.K. Leiros, J. Timmins, R.B. Ravelli, S.M. McSweeney, Is radiation damage dependent on the dose rate used during macromolecular crystallography data collection? Acta Crystallogr. D Biol. Crystallogr. 62 (2006) 125–132.
[90] R.H. Baxter, B.L. Seagle, N. Ponomarenko, J.R. Norris, Specific radiation damage illustrates light-induced structural changes in the photosynthetic reaction center, J. Am. Chem. Soc. 126 (2004) 16728–16729.
[91] A. Royant, M. Noirclerc-Savoye, Stabilizing role of glutamic acid 222 in the structure of Enhanced Green Fluorescent Protein, J. Struct. Biol. 174 (2011) 385–390.
[92] A.P. Dubnovitsky, R.B. Ravelli, A.N. Popov, A.C. Papageorgiou, Strain relief at the active site of phosphoserine aminotransferase induced by radiation damage, Protein Sci. 14 (2005) 1498–1507.
[93] M. Andersson, E. Malmerberg, S. Westenhoff, G. Katona, M. Cammarata, A.B. Wohri, L.C. Johansson, F. Ewald, M. Eklund, M. Wulff, J. Davidsson, R. Neutze, Structural dynamics of light-driven proton pumps, Structure 17 (2009) 1265–1275.
[94] M.H. Koch, N.A. Dencher, D. Oesterhelt, H.J. Plohn, G. Rapp, G. Buldt, Time-resolved X-ray diffraction study of structural changes associated with the photocycle of bacteriorhodopsin, EMBO J. 10 (1991) 521–526.
[95] H. Kamikubo, T. Oka, Y. Imamoto, F. Tokunaga, J.K. Lanyi, M. Kataoka, The last phase of the reprotonation switch in bacteriorhodopsin: the transition between the M-type and the N-type protein conformation depends on hydration, Biochemistry 36 (1997) 12282–12287.
[96] T. Oka, H. Kamikubo, F. Tokunaga, J.K. Lanyi, R. Needleman, M. Kataoka, Conformational change of helix G in the bacteriorhodopsin photocycle: investigation with heavy atom labeling and x-ray diffraction, Biophys. J. 76 (1999) 1018–1023.
[97] N.A. Dencher, D. Dresselhaus, G. Zaccai, G. Buldt, Structural changes in bacteriorhodopsin during proton translocation revealed by neutron diffraction, Proc. Natl. Acad. Sci. U. S. A. 86 (1989) 7876–7879.
[98] S. Subramaniam, M. Gerstein, D. Oesterhelt, R. Henderson, Electron diffraction analysis of structural changes in the photocycle of bacteriorhodopsin, EMBO J. 12 (1993) 1–8.
[99] M. Andersson, J. Vincent, D. van der Spoel, J. Davidsson, R. Neutze, A proposed time-resolved X-ray scattering approach to track local and global conformational changes in membrane transport proteins, Structure 16 (2008) 21–28.
[100] M. Cammarata, M. Levantino, F. Schotte, P.A. Anfinrud, F. Ewald, J. Choi, A. Cupane, M. Wulff, H. Ihee, Tracking the structural dynamics of proteins in solution using time-resolved wide-angle X-ray scattering, Nat. Methods 5 (2008) 881–886.
[101] E. Malmerberg, Z. Omran, J.S. Hub, X. Li, G. Katona, S. Westenhoff, L.C. Johansson, M. Andersson, M. Cammarata, M. Wulff, D. van der Spoel, J. Davidsson, A. Specht, R. Neutze, Time-resolved WAXS reveals accelerated conformational changes in iodoretinal-substituted proteorhodopsin, Biophys. J. 101 (2011) 1345–1353.
[102] T.W. Kim, J.H. Lee, J. Choi, K.H. Kim, L.J. van Wilderen, L. Guerin, Y. Kim, Y.O. Jung, C. Yang, J. Kim, M. Wulff, J.J. van Thor, H. Ihee, Protein structural dynamics of

photoactive yellow protein in solution revealed by pump-probe X-ray solution scattering, J. Am. Chem. Soc. 134 (2012) 3145–3153.
[103] K.H. Kim, S. Muniyappan, K.Y. Oang, J.G. Kim, S. Nozawa, T. Sato, S.Y. Koshihara, R. Henning, I. Kosheleva, H. Ki, Y. Kim, T.W. Kim, J. Kim, S.I. Adachi, H. Ihee, Direct Observation of Cooperative Protein Structural Dynamics of Homodimeric Hemoglobin from 100 ps to 10 ms with Pump-Probe X-ray Solution Scattering, J. Am. Chem. Soc. 134 (2012) 7001–7008.
[104] M. Sheves, A. Albeck, N. Friedman, M. Ottolenghi, Controlling the pKa of the bacteriorhodopsin Schiff base by use of artificial retinal analogues, Proc. Natl. Acad. Sci. U. S. A. 83 (1986) 3262–3266.
[105] C.H. Chang, R. Jonas, R. Govindjee, T.G. Ebrey, Regeneration of blue and purple membranes from deionized bleached membranes of Halobacterium halobium, Photochem. Photobiol. 47 (1988) 261–265.
[106] Y. Gat, M. Sheves, A mechanism for controlling the pKa of the retinal protonated Schiff base in retinal proteins. A study with model compounds, J. Am. Chem. Soc. 115 (1993) 3772–3773.
[107] A.N. Bondar, J. Baudry, S. Suhai, S. Fischer, J.C. Smith, Key role of active-site water molecules in bacteriorhodopsin proton-transfer reactions, J. Phys. Chem. B 112 (2008) 14729–14741.
[108] A.N. Bondar, S. Fischer, J.C. Smith, M. Elstner, S. Suhai, Key role of electrostatic interactions in bacteriorhodopsin proton transfer, J. Am. Chem. Soc. 126 (2004) 14668–14677.
[109] H.G. Khorana, Two light-transducing membrane proteins: bacteriorhodopsin and the mammalian rhodopsin, Proc. Natl. Acad. Sci. U. S. A. 90 (1993) 1166–1171.
[110] J. Tittor, S. Paula, S. Subramaniam, J. Heberle, R. Henderson, D. Oesterhelt, Proton translocation by bacteriorhodopsin in the absence of substantial conformational changes, J. Mol. Biol. 319 (2002) 555–565.
[111] H. Luecke, B. Schobert, J. Stagno, E.S. Imasheva, J.M. Wang, S.P. Balashov, J.K. Lanyi, Crystallographic structure of xanthorhodopsin, the light-driven proton pump with a dual chromophore, Proc. Natl. Acad. Sci. U. S. A. 105 (2008) 16561–16565.
[112] I. Gushchin, P. Chervakov, P. Kuzmichev, A.N. Popov, E. Round, V. Borshchevskiy, A. Ishchenko, L. Petrovskaya, V. Chupin, D.A. Dolgikh, A.S. Arseniev, M. Kirpichnikov, V. Gordeliy, Structural insights into the proton pumping by unusual proteorhodopsin from nonmarine bacteria, Proc. Natl. Acad. Sci. U. S. A. 110 (2013) 12631–12636.
[113] K. Yoshimura, T. Kouyama, Structural role of bacterioruberin in the trimeric structure of archaerhodopsin-2, J. Mol. Biol. 375 (2008) 1267–1281.
[114] A. Royant, P. Nollert, K. Edman, R. Neutze, E.M. Landau, E. Pebay-Peyroula, J. Navarro, X-ray structure of sensory rhodopsin II at 2.1-A resolution, Proc. Natl. Acad. Sci. U. S. A. 98 (2001) 10131–10136.
[115] J. Sasaki, J.L. Spudich, Proton transport by sensory rhodopsins and its modulation by transducer-binding, Biochim. Biophys. Acta 1460 (2000) 230–239.
[116] E.N. Spudich, G. Ozorowski, E.V. Schow, D.J. Tobias, J.L. Spudich, H. Luecke, A transporter converted into a sensor, a phototaxis signaling mutant of bacteriorhodopsin at 3.0 A, J. Mol. Biol. 415 (2012) 455–463.
[117] H. Sato, K. Takeda, K. Tani, T. Hino, T. Okada, M. Nakasako, N. Kamiya, T. Kouyama, Specific lipid-protein interactions in a novel honeycomb lattice structure of bacteriorhodopsin, Acta Crystallogr. D Biol. Crystallogr. 55 (1999) 1251–1256.
[118] H.J. Sass, G. Buldt, R. Gessenich, D. Hehn, D. Neff, R. Schlesinger, J. Berendzen, P. Ormos, Structural alterations for proton translocation in the M state of wild-type bacteriorhodopsin, Nature 406 (2000) 649–653.
[119] M.T. Facciotti, V.S. Cheung, D. Nguyen, S. Rouhani, R.M. Glaeser, Crystal structure of the bromide-bound D85S mutant of bacteriorhodopsin: principles of ion pumping, Biophys. J. 85 (2003) 451–458.
[120] M.T. Facciotti, V.S. Cheung, C.S. Lunde, S. Rouhani, N.S. Baliga, R.M. Glaeser, Specificity of anion binding in the substrate pocket of bacteriorhodopsin, Biochemistry 43 (2004) 4934–4943.
[121] S. Faham, D. Yang, E. Bare, S. Yohannan, J.P. Whitelegge, J.U. Bowie, Side-chain contributions to membrane protein structure and stability, J. Mol. Biol. 335 (2004) 297–305.
[122] S. Yohannan, S. Faham, D. Yang, J.P. Whitelegge, J.U. Bowie, The evolution of transmembrane helix kinks and the structural diversity of G protein-coupled receptors, Proc. Natl. Acad. Sci. U. S. A. 101 (2004) 959–963.
[123] S. Yohannan, S. Faham, D. Yang, D. Grosfeld, A.K. Chamberlain, J.U. Bowie, A C alpha-H…O hydrogen bond in a membrane protein is not stabilizing, J. Am. Chem. Soc. 126 (2004) 2284–2285.
[124] S. Yohannan, D. Yang, S. Faham, G. Boulting, J. Whitelegge, J.U. Bowie, Proline substitutions are not easily accommodated in a membrane protein, J. Mol. Biol. 341 (2004) 1–6.
[125] N.H. Joh, A. Min, S. Faham, J.P. Whitelegge, D. Yang, V.L. Woods, J.U. Bowie, Modest stabilization by most hydrogen-bonded side-chain interactions in membrane proteins, Nature 453 (2008) 1266–1270.
[126] N.H. Joh, A. Oberai, D. Yang, J.P. Whitelegge, J.U. Bowie, Similar energetic contributions of packing in the core of membrane and water-soluble proteins, J. Am. Chem. Soc. 131 (2009) 10846–10847.
[127] Z. Cao, J.U. Bowie, Shifting hydrogen bonds may produce flexible transmembrane helices, Proc. Natl. Acad. Sci. U. S. A. 109 (2012) 8121–8126.
[128] S. Wolf, E. Freier, M. Potschies, E. Hofmann, K. Gerwert, Directional proton transfer in membrane proteins achieved through protonated protein-bound water molecules: a proton diode, Angew. Chem. Int. Ed. Engl. 49 (2010) 6889–6893.
[129] V. Borshchevskiy, E. Moiseeva, A. Kuklin, G. Bueldt, M. Hato, V. Gordeliy, Isoprenoid-chained lipid β-XylOC$_{16+4}$—a novel molecule for *in meso* membrane protein crystallization, J. Cryst. Growth 312 (2010) 3326–3330.
[130] S.C. Lee, B.C. Bennett, W.X. Hong, Y. Fu, K.A. Baker, J. Marcoux, C.V. Robinson, A.B. Ward, J.R. Halpert, R.C. Stevens, C.D. Stout, M.J. Yeager, Q. Zhang, Steroid-based facial amphiphiles for stabilization and crystallization of membrane proteins, Proc. Natl. Acad. Sci. U. S. A. 110 (2013) E1203–1211.